DIRC-based PID for the EIC Central Detector

T. Cao[3], T. Horn[1] (co-PI), C. Hyde[2] (co-PI), Y. Ilieva[3] (co-PI), P. Nadel-Turonski[4,*] (co-PI), K. Peters[5], C. Schwarz[5], J. Schwiening[5] (co-PI), H. Seraydaryan[2], W. Xi[4], C. Zorn[4].

[1)] The Catholic University of America, Washington, DC 20064
[2)] Old Dominion University, Norfolk, VA 23529
[3)] University of South Carolina, Columbia, SC 29208
[4)] Thomas Jefferson National Accelerator Facility, Newport News, VA 23606
[5)] GSI Helmholtzzentrum für Schwerionenforschung GmbH, 64291 Darmstadt, Germany
[*)] turonski@jlab.org

Abstract

An essential requirement for the central detector of an Electron-Ion Collider (EIC) is a radially-compact subsystem providing particle identification (e/π, π/K, K/p) over a wide momentum range. To this end, the electromagnetic calorimeter needs to be complemented by one or more Cherenkov detectors. With a radial size of only a few cm, a Detector of Internally Reflected Cherenkov light (DIRC) is a very attractive option. Currently, R&D is being undertaken for several DIRC projects around the world (Belle-II, PANDA, LHCb). A future EIC DIRC can benefit from many aspects of this R&D, but it also provides its own unique set of challenges and priorities, in particular due to the higher momenta of the produced particles, and the impact of the readout of the DIRC bars on the required detector acceptance.

The key questions addressed by the proposed R&D include: developing a compact readout "camera" that can operate in the high magnetic fields, investigating the possibility to extend the momentum coverage (up to 50% beyond state-of-the-art for π/K identification) by improving the θ_c resolution, and studying the integration of a DIRC into the EIC full-acceptance detector.

This proposal is currently in its second year of funding. The first year has yielded some very important results, including simulations showing a proof-of-principle for achieving the θ_c resolution that was set out as the original goal for our investigation, but further work on simulations and hardware is needed. In order to capitalize on our findings, and due to unavailability of suitable test beams during Year 3, we are proposing to extend the R&D effort into Year 4, but with reduced annual expenditures, in particular on hardware. This would delay the construction of the final prototype by one year, but makes it possible to incorporate all of our findings, both from simulations and sensor tests.

Table of Contents

1. Physics Requirements for Large-Angle Particle Identification
    1.1 π/K identification
        1.1.1 Semi-Inclusive DIS and Transverse Momentum Distributions (TMDs)
        1.1.2 Exclusive meson production and Generalized Parton Distributions (GPDs)
    1.2 e/π identification
    1.3 Implications for PID and DIRC performance
2. PID in the EIC Central Detector
    2.1 General layout of the EIC central detector
    2.2 Brief overview of PID options
    2.3 Solenoid options
    2.4 DIRC configurations with readout inside of the solenoid
    2.5 DIRC configurations with readout outside of the solenoid
    2.6 Accelerator background
3. DIRC detectors
    3.1 Principle
    3.2 Contributions to the Cherenkov angle (θc) resolution
    3.3 Adaptation to EIC requirements
        3.3.1 Size of expansion volume
        3.3.2 Small-pixel readout
        3.3.3 Increasing the photon yield
        3.3.4 Sensor performance in magnetic fields
        3.3.5 Precision timing
4. Proposed R&D
    4.1 General Goals
    4.2 Detector simulations
        4.2.1 GEANT
        4.2.2 Configurations with expansion volume inside solenoid
        4.2.3 Configurations with expansion volume outside of solenoid
        4.2.4 Prototype configuration
    4.3 Sensor tests
        4.3.1 Gain studies at high-B field test facility at JLab
            4.3.1.1 Facility description
            4.3.1.2 Planned tests and Procedures
            4.3.1.3 Broader impact
        4.3.2 Timing studies at GSI
        4.3.3 Radiation hardness
    4.4 Prototyping
        4.4.1 Lens with high refractive index
        4.4.2 Compact expansion volume
        4.4.3 Sensors and DAQ
        4.4.4 In-beam tests

4.5 Synergies
5. R&D Timeline and Deliverables
5.1 Timeline
5.1.1 Year 1
5.1.2 Year 2
5.1.3 Year 3
5.1.4 Year 4
5.2 Deliverables
5.2.1 Year 1
5.2.2 Year 2
5.2.3 Year 3
5.2.4 Year 4
6. Management Plan
6.1 Funding Request and Budget
6.2 Procurement
6.3 Responsibilities

1. Physics Requirements for Large-Angle Particle Identification

1.1 π/K identification

While an EIC could support multiple interaction regions, the primary detector will have a general-purpose character that should offer satisfactory performance for a wide range of processes and kinematics. In practice, however, the most stringent particle identification (PID) requirements for the central detector come from semi-inclusive and exclusive reactions.

As shown in Fig. 1, the inclusive momentum distribution of all hadrons produced at central angles in (inclusive) Deep Inelastic Scattering (DIS), is dominated by particles well below 4 GeV/c. Of particular note, higher ion beam energies (right-hand panel) primarily impact the momentum distribution at very forward angles, and have limited impact on the inclusive distributions in the central region. On the other hand, these soft distributions are only obtained if no additional kinematical constraints are applied (*e.g.*, cuts on x — the momentum fraction carried by the struck quark, Q^2 — the photon virtuality, or z — the fraction of jet energy in detected parton, etc.).

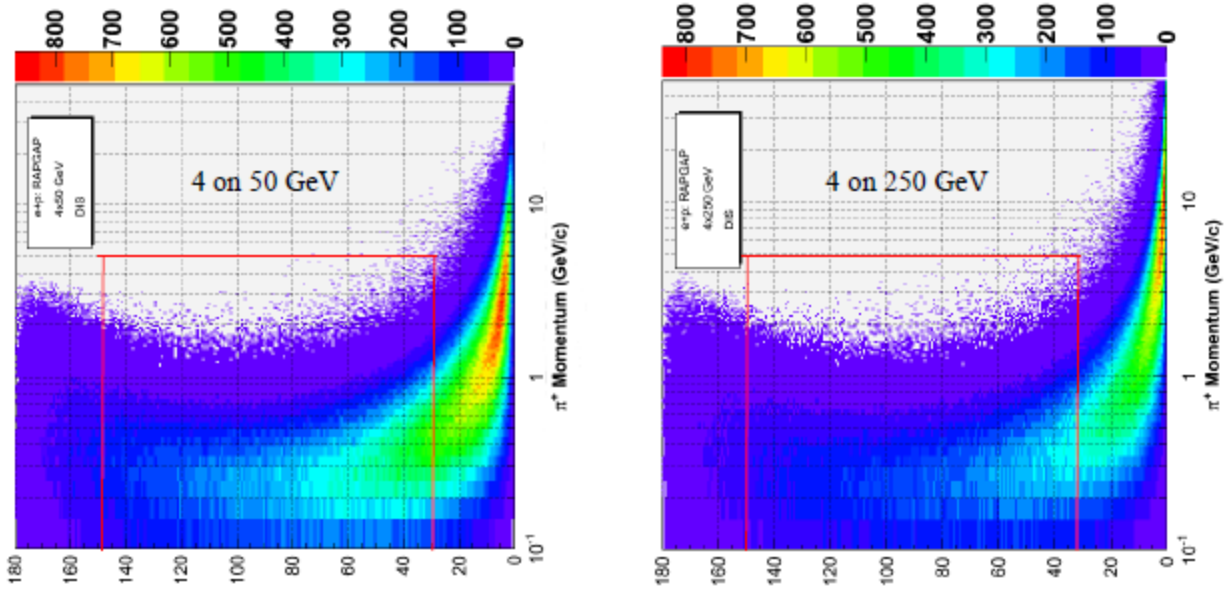

Figure 1: DIS pions produced in collisions of 4 GeV electrons on 50 GeV and 250 GeV protons, respectively. The vertical red lines placed at 30° and 150° indicate the approximate transition from the central detector to the endcaps. The horizontal line at 4 GeV/c shows the limit of 3σ π/K separation for current DIRC detectors. No cuts on Q^2 have been applied in the plots. Note that in the HERA convention the electron beam is moving towards 180° (*i.e.*, towards the left) and the ion beam is moving towards 0° (*i.e.*, towards the right).

However, the more exclusive the process, the larger the fraction of the reaction momentum that is picked up by the leading hadron emerging from the struck quark. This fraction is called z, and in the exclusive case, where only one hadron is produced, $z \rightarrow 1$. For such events, higher ion beam energies cannot translate into a larger number of created particles, and the kinematic boost is thus more marked. The large-z limit thus poses the greatest challenge for detection and particle identification, in particular at

forward angles, but also for the central detector. This is illustrated in Fig. 2, which shows the variation of semi-inclusive hadron momenta (polar angle θ_h and modulus p) constrained by contours of either constant Q^2 (variable x) or constant x (variable Q^2). Note that for each (Q^2, x, θ_h) point, the momentum of the hadron scales with z. For example, at $x = 0.1$, the jet energy (in the collider frame) is approximately 10 GeV for all but the very highest Q^2. Thus, detecting pions and kaons at $z = 0.5$ requires PID up to 5 GeV/c. Similarly, exclusive meson production ($z \rightarrow 1$) at $x = 0.05$ will also require PID up to 5 GeV/c. This includes for example, exclusive φ-production, because it is important to detect both symmetric and asymmetric φ → KK decays.

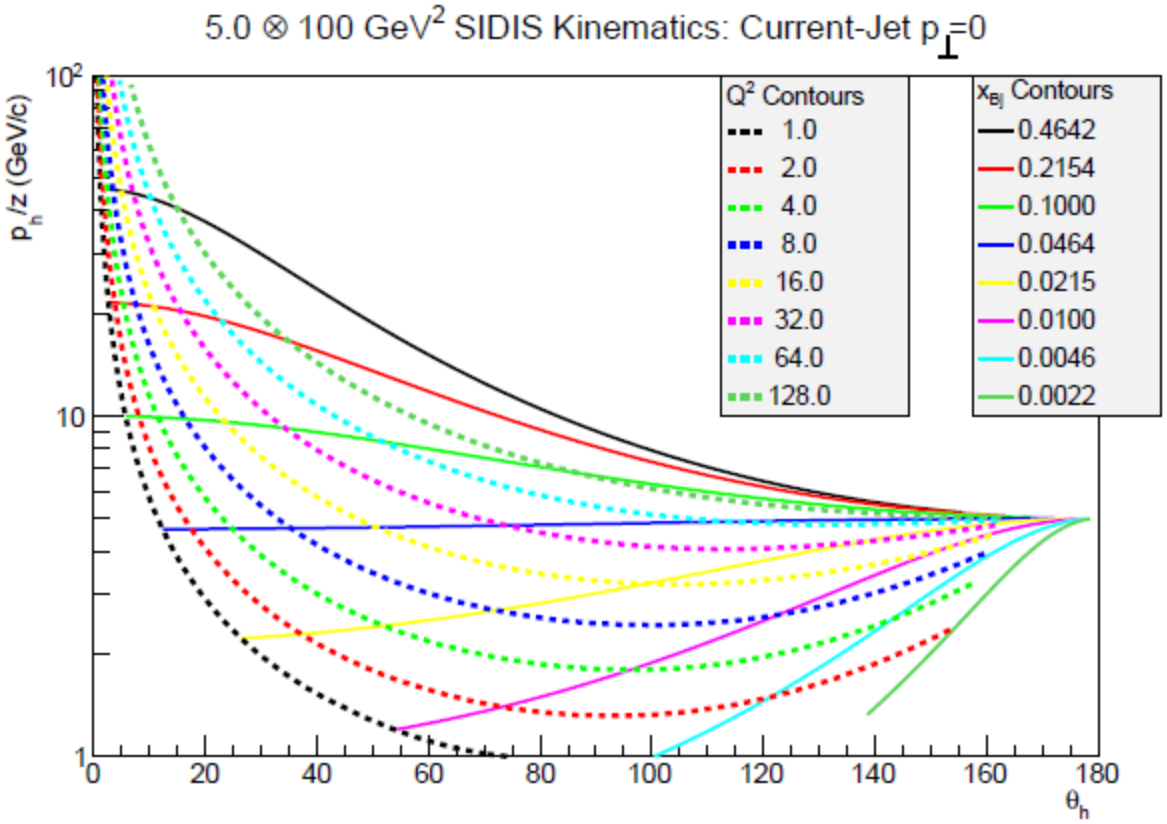

Figure 2: Momentum *vs.* polar angle distribution for SIDIS mesons with a certain z, x, and Q^2, produced at small p_T. Here, zero degrees is in the direction of the outgoing ion beam (to the left in the figure). Note that the momentum axis is scaled by z. The plot illustrates how improving the momentum coverage of the DIRC makes it possible to extend the coverage in x and Q^2, and that extending the momentum reach is most important at the forward angles. The central detector spans a range roughly from 30° to 150°.

1.1.1 Semi-Inclusive DIS and Transverse Momentum Distributions (TMDs)

As the name suggests, Semi-Inclusive Deep Inelastic Scattering (SIDIS) lies somewhere in-between inclusive DIS and exclusive processes. On one hand, it can simply involve tagging a hadron in coincidence with the scattered electron. On the other, multi-dimensional measurements of the leading hadron make it possible to map out the 3D partonic structure of the nucleon in momentum space through Transverse

Momentum Distributions (TMDs), and could provide access to the quark orbital angular momentum, which is thought to have a large contribution to the spin of the proton. Here, one wants to map a broad range in z, x, and Q^2, making TMD measurements a good benchmark for PID.

In addition to x, Q^2, and z, SIDIS structure functions in general, and TMDs in particular, are also characterized by the intrinsic transverse momentum of the struck quark (k_T), and the transverse momentum of the produced hadron (p_T), where only the latter is an observable. Ideally, just as with z, one would like to map out the p_T-dependence over the full kinematic range. Unfortunately, since the EIC will cover a very considerable range in p_T, although it would have been desirable, it is not feasible to provide PID for all kinematics, in particular in the central detector where space is limited. Nevertheless, the PID can be sufficiently good to address some key physics questions. This is easiest to see in the context of the p_T-coverage.

To learn about nucleon structure, the scattering process is factorized into a hard part that can be calculated perturbatively, and a soft part that carries the information about the nucleon. Two different factorization schemes exist. The traditional, collinear factorization scheme applies when the p_T of the produced hadron is of order Q, and the intrinsic k_T of the quarks inside the nucleon can be neglected. The transverse momentum of the produced hadron (p_T), then reflects the dynamics of the process. In the collinear picture, one would like to study p_T over a range similar to that in Q.

However, if one wants to learn about the 3D partonic structure of the nucleon, and ultimately the orbital angular momentum, the transverse momentum k_T becomes important. A different factorization scheme is required to include k_T explicitly. It is known as TMD factorization, and applies when $p_T \sim \Lambda_{QCD} << Q^2$. Thus, three regimes exist: one at high p_T where collinear factorization applies, one at low p_T where TMD factorization applies, and a transition region in-between, which should be well described by both. To successfully study the 3D structure of the nucleon in momentum space, it is necessary to be able to simultaneously cover all three. To do so one will need to identify kaons over the largest possible momentum range.

Employing polarized beams, the EIC will be able to study a number of TMDs. Each TMD represents different combination of spin and quark momentum correlations. One of the simplest TMDs, called the Sivers function, was suggested at the INT 10-3 program as a golden measurement for an EIC. The k_T-distribution for the Sivers function is shown in Fig 3.

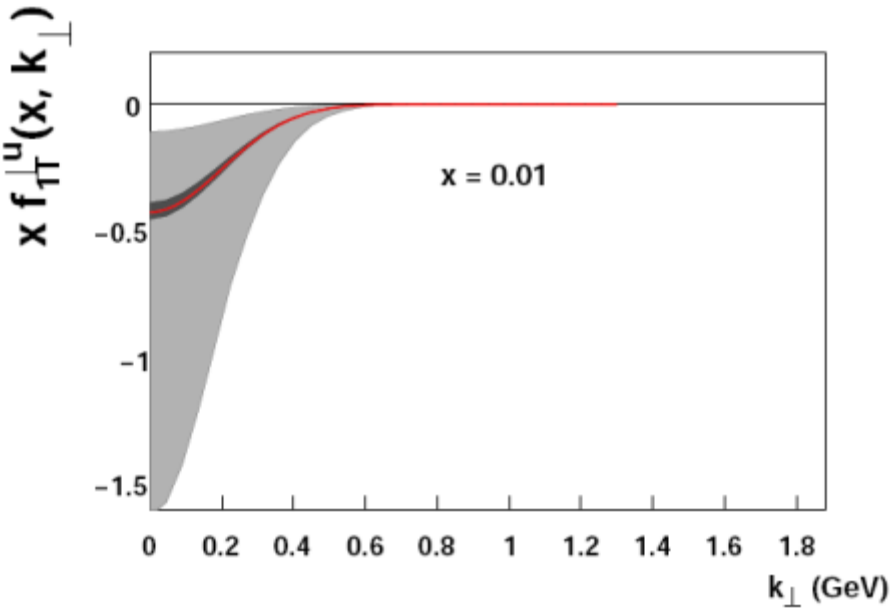

Figure 3: Dependence of the Sivers function on the transverse quark momentum. The light and dark grey bands are estimates of the uncertainty before and after EIC data become available, respectively.

The distribution shows the three regions of interest. As expected from the natural momentum scale associated with the nucleon, TMDs are large only at low values of k_T (and hence low to moderate p_T). Although the shape of the TMDs may change with x, they will fall off rapidly at large k_T for all values of x. By splitting up k_T into its components, we obtain an image in the transverse plane (with respect to the virtual photon direction). Figure 4 shows how the incoming photon "sees" the motion of the quarks.

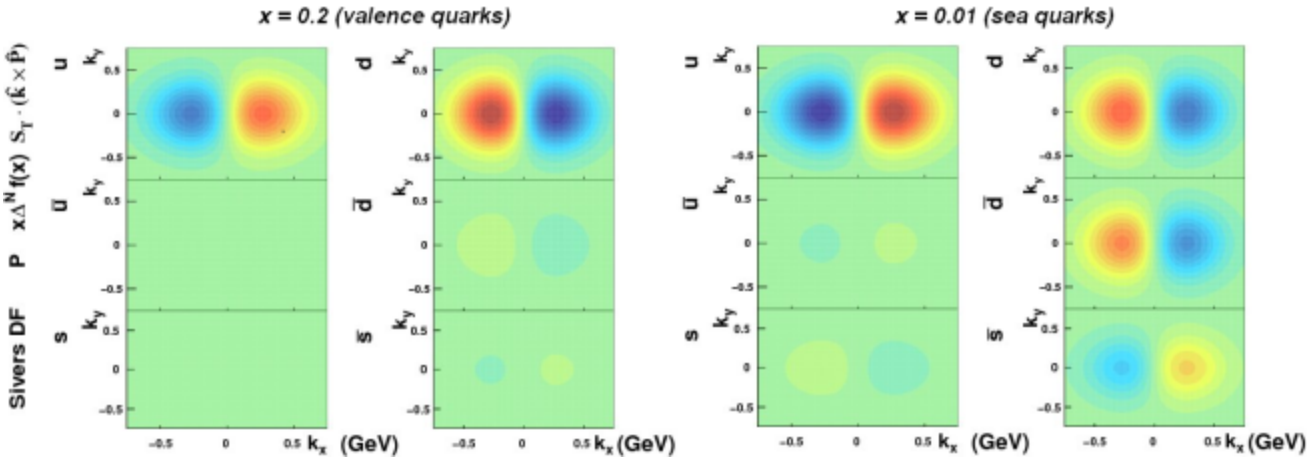

Figure 4: Sivers function for u, d, and s quarks (as well as antiquarks) as function of the transverse quark momentum components as "seen" by the incoming photon. Red indicates an excess and blue a depletion. Flavor separation will require π/K identification.

However, one needs to keep in mind that, depending on the kinematics of the process, p_T is usually larger than k_T. In order to disentangle the two, the measured range in p_T has to significantly exceed the desired range in k_T. In addition, both k_T and p_T are defined in the ion rest frame with respect to the virtual photon direction (rather than that of the ion beam). The p_T in the lab frame is thus boosted along the beam direction, and tends to differ from the p_T in the target rest frame. And finally, due to the boost and the meson scattering angle, the lab momentum p, which is the parameter determining the coverage of the PID detectors, is almost invariably larger than the p_T in the ion rest frame (thus, since the PID is limited by p, the coverage in k_T is better at lower ion beam energies). An example of the lab angles and momenta as function of p_T for the SIDIS leading hadron at intermediate collision energies is shown in Fig. 5.

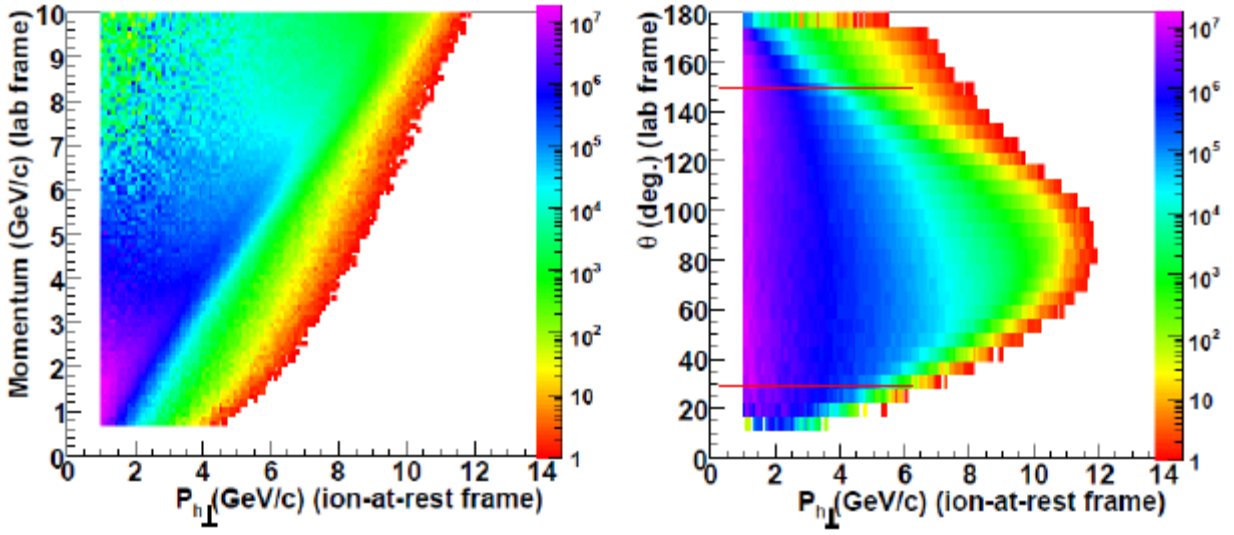

Figure 5: Leading SIDIS pions for 11 GeV electrons on 60 GeV protons, with cuts on $0.2 < z < 0.8$, $Q^2 > 1$ GeV^2, $M_x > 1.6$ GeV, $W > 2.3$ GeV, $0.05 < y < 0.8$, and $p < 10$ GeV, as function of p_T. The horizontal red lines indicate the approximate transition from the central detector to the endcaps.

The corresponding SIDIS lab momenta as a function of angle are shown in Fig. 6. The left panel focuses on the central detector, indicating the coverage of a DIRC (both state-of-the-art and a high-performance "Super-DIRC"). The right panel shows the distribution of forward-going particles, the momenta of which are driven by the ion beam energy. Due to the lower electron energy in the right panel, the momenta of backward-going mesons are lower than on the left panel.

To summarize, one would like to have the EIC detector provide flavor separation over the full range of p_T accessible in SIDIS. However, for studies of TMDs such as the Sivers function, one needs to cover a range in p_T that will make it possible to disentangle the lower end of the k_T distribution and the hitherto

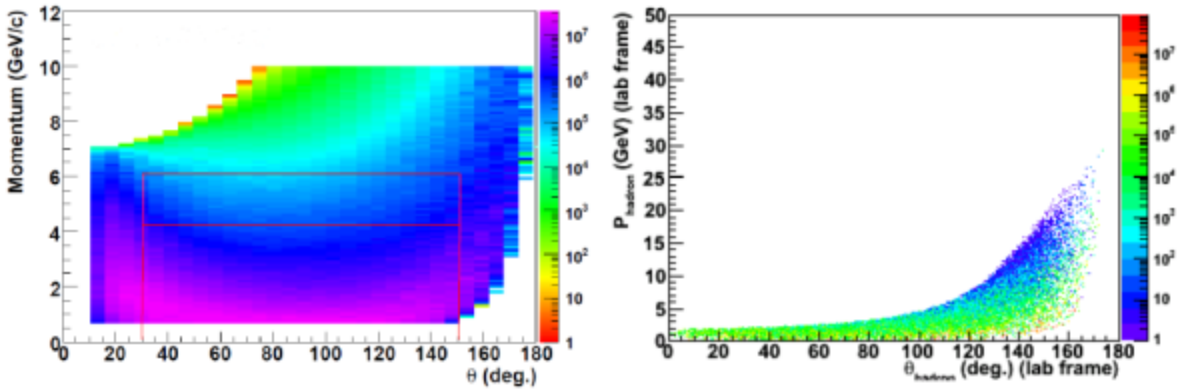

Figure 6: Leading SIDIS pions for 11 GeV electrons on 60 GeV protons (left panel) and 4 GeV electrons on 50 GeV protons (right panel). In the left panel the same cuts have been applied as in Fig. 5, while on the right, $0.4 < z < 0.6$ and $1 < Q^2 < 10$ GeV^2. The horizontal red lines at 4 and 6 GeV/c indicate, respectively, the 3σ π/K separation of a state-of-the-art DIRC and a the upper limit of a possible "Super-DIRC". Note that these and subsequent plots use the standard electron scattering convention where the electron beam moves towards 0°. The left/right directions of the electron/ion beams are, however, the same as in Fig. 1.

unknown transition region at intermediate p_T (and high k_T) where both TMD- and collinear factorization are relevant, as well as the lower portion of the high-p_T collinear region. Accomplishing this would require a slightly larger momentum coverage, in particular at the more forward angles covered by the central detector, than could be achieved by the BaBar DIRC, for instance using a high-performance DIRC or aerogel RICH. Further extending the coverage from 5 - 6 GeV/c to 9 GeV/c using a gas Cherenkov (threshold or as part of a dual-radiator RICH) would require at least 60 - 70 cm of radial space in addition to the few cm needed for the DIRC (or a somewhat thicker aerogel RICH). Since the 5 - 6 GeV/c range would be sufficient for covering the three regions above for relevant kinematics, while 9 GeV/c would still fall short of the full kinematic coverage of the EIC, the latter does not constitute an appealing option overall. The focus of this proposal is thus to present a solution that could accommodate the PID needs of the TMD program, and provide a substantial coverage of the general SIDIS kinematics.

1.1.2 Exclusive meson production and Generalized Parton Distributions (GPDs)

Measurements of the transverse spatial parton distributions, using the GPD framework, are complementary to the 3D imaging in momentum space discussed in the previous section. Experimentally, the exclusive sector is more complicated in that one not only needs to detect and identify the meson originating from the struck quark, but one would like to use a suite of diffractive and non-diffractive processes (diffractive implies no change in quantum numbers, *e.g.*, for DVCS, φ, and J/Ψ, while non-diffractive, *e.g.*, π, K, ρ^+, does). Figure 7 illustrates what can be learned from comparison of parton distributions in transverse impact-parameter space, measured in different channels.

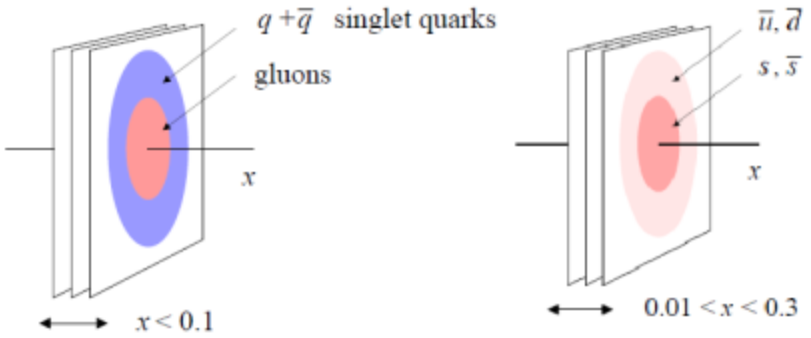

Figure 7: A comparison between DVCS and J/Ψ production, for example, can teach us about the relative quark and gluon radii of hadrons, while a comparison between pions and kaons (or non-diffractive vector meson channels) can provide information about the relative distributions of light and strange sea quarks.

Detection and PID challenges vary from channel to channel. Decaying mesons split their momentum between the decay products, and often have a relatively narrow invariant mass (*e.g.*, $\varphi \rightarrow K^+K^-$). Most difficult to identify are long-lived pseudoscalars such as the kaon, for which the lab momenta become large already at relatively low lab energies. On the other hand, since the cross sections for non-diffractive processes fall with energy, providing sufficient PID to cover the lower end of the energy range will be adequate. Figure 8 shows the angular distribution of exclusive light mesons at several center-of-mass (c.m.) collision energies, all with a high Q^2 (> 10 GeV^2) cut applied.

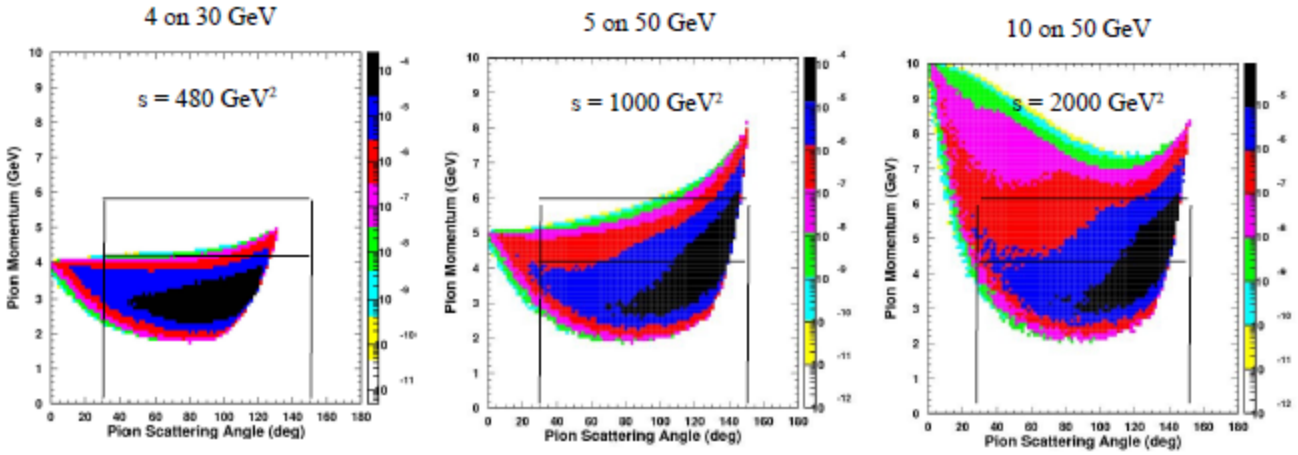

Figure 8: Exclusive pion production at Q^2 > 10 GeV^2 for three kinematics: 4 on 30, 5 on 50, and 10 on 50 GeV. As indicated by the horizontal lines, π/K identification up to 4 GeV/*c* is sufficient at the lowest c.m. energies, but quickly becomes inadequate as the energy increases.

A momentum coverage up to 4 GeV/*c* (state-of-the-art DIRC) is only adequate for very low values of *s*. Increasing this value to 6 GeV/*c* would provide full coverage up to s = 2000 GeV^2, if the collision kinematics are reasonably symmetric, and partial coverage for higher energies.

1.2 e/π identification

When studying electron scattering, a reliable electron identification is essential. In the endcaps this can be

accomplished using both the electromagnetic calorimeter as well as gas Cherenkov detectors for e/π identification. However, in the barrel region there will only be an electromagnetic calorimeter. This will be sufficient in kinematics where the momentum of the scattered electron is high, but at low momenta the pion background becomes significant. Here a high-performance DIRC can provide the additional PID capability needed to push to lower electron momenta. This can be important for determining F_L, as well as for other measurements that wish to cover a wide range of photon virtualities (Q^2) and electron inelasticities (y). As shown in Fig. 9, a DIRC makes it possible to reach higher values of Q^2 at low x.

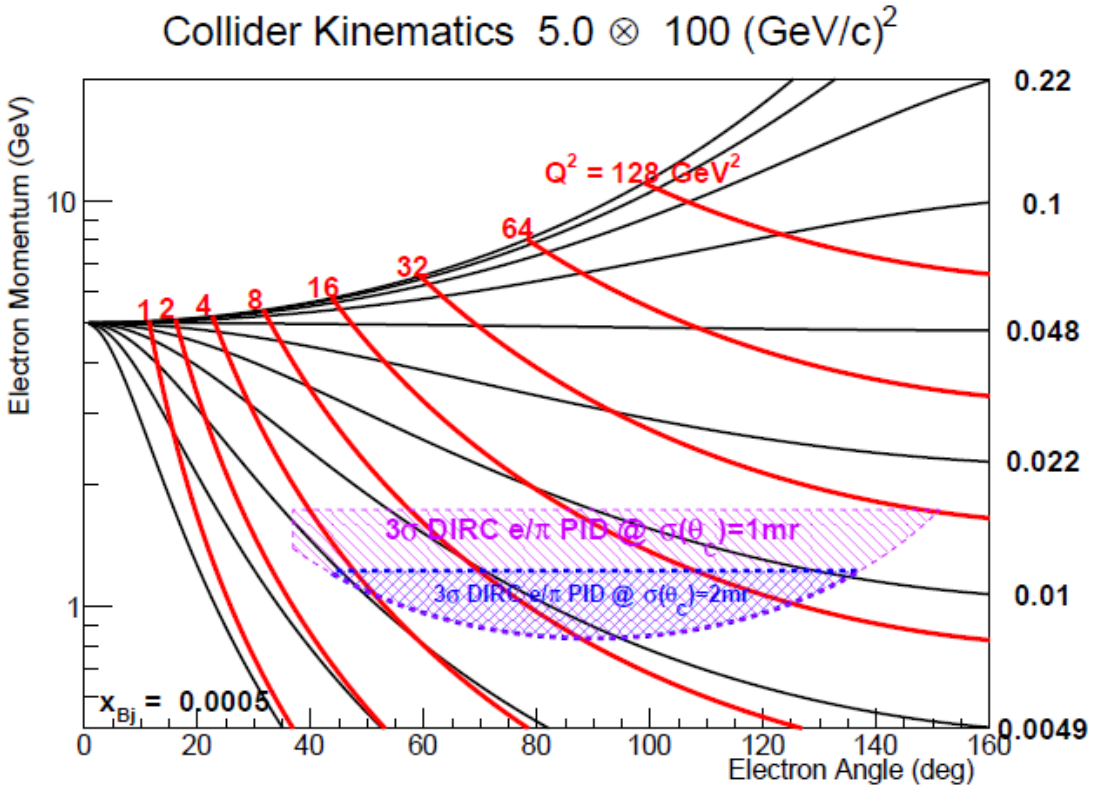

Figure 9: Electron kinematics showing the range where a DIRC could contribute to the e/π identification, and the benefit of extending its momentum coverage. The lower limit is determined by the requirement that the particle track in a 3-Tesla solenoid field extends through the DIRC and TOF counters to the central EM calorimeters. In this plot, zero degrees refers to the outgoing electron beam direction.

1.3 Implications for PID and DIRC performance

The PID requirements are primarily driven by semi-inclusive and exclusive processes requiring large z and p_T. There is no feasible way of extending the π/K identification over the full kinematics that will be studied at the EIC. However, a high-performance DIRC could provide adequate coverage for studies of the 3D structure of the nucleon in both momentum (TMDs) and coordinate (GPDs) space. Due to the boost in the ion direction, it is highly desirable to have the best resolution at the forward angles. The impact of particle multiplicities on the azimuthal segmentation needs to be studied. The improved e/π identification could also extend the Q^2-coverage at low x.

2. PID in the EIC Central Detector

2.1 General layout of the EIC central detector

Although there are some minor differences in the layout of the detectors envisioned at JLab and BNL, driven in part by the space available in the IR, the general features and requirements are similar. This is, in particular, true for the layout of the detectors in the solenoid barrel. Here, the constraints on the radial space budget only allow a limited number of options. As shown in Figures 10 and 11, the consensus is to use a compact EM calorimeter, (for instance using tungsten powder, a technology also funded by the generic R&D program, or lead and scintillating fibers, with readout on both ends, as used for the GlueX experiment at JLab). Hadronic PID would be provided by a compact ring imaging Cherenkov detector - either a DIRC or proximity-focused aerogel. The JLab detector sketch also explicitly includes a high-precision time-of-flight detector. Ongoing R&D shows that time resolutions of 10 ps or better could be achieved, which would be very attractive for a collider operating with ps-long bunches providing a clear time definition in a single layer, even though the flight path in the barrel is short. However, a precise determination of the hit time would also facilitate event reconstruction in the DIRC, and a DIRC + TOF combination would still be radially more compact than an aerogel RICH. From the DIRC point of view, it is also important that the tracker can provide an angular resolution as good or better than the Cherenkov angle resolution of the DIRC. This should be possible to achieve with GEMs, which perhaps can be regarded as the baseline technology for the central tracker, although a digital TPC (like the one proposed for the ILD detector, or hybrid based on the PHENIX HBD for which R&D is being performed), or an ultra-low mass cluster-counting drift chamber (as was proposed for the 4th concept detector for the ILC) should also be able to achieve such performance. In terms of hadronic calorimetry, there are several interesting HEP R&D projects such as the RD52 (dual-readout) and particle-flow concepts, but high resolution requires many interaction lengths. Such technologies would be prime candidates for neutron detection in the zero-degree calorimeter (ZDC), but it is difficult to motivate the cost of adding a 2-m thick hadronic calorimeter to a relatively small central detector (compared with HEP projects) as the one envisioned by the EIC, in particular since it is not critical for carrying out the envisioned physics program.

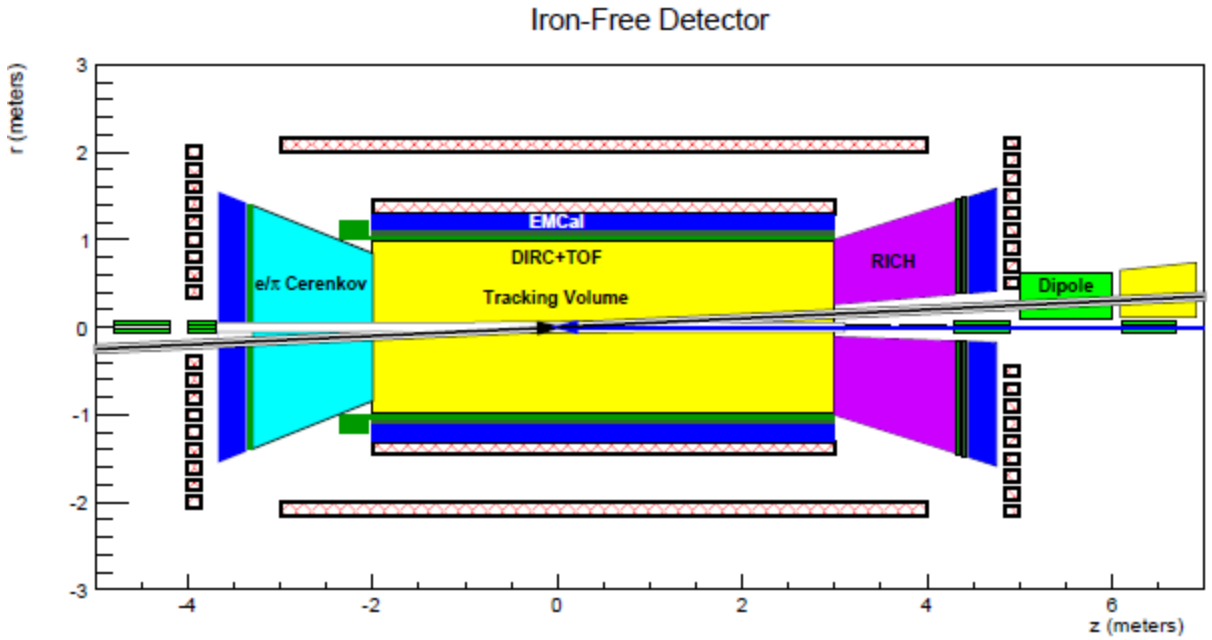

Figure 10: Top view of an initial JLab concept based on a 3T iron-free dual solenoid providing easy access and a lot of space for the endcap detectors. Normal-conducting coils behind the endcaps remove the longitudinal fringe fields. Electron quads are down in green (the ion quads are outside of the picture). The figure shows one possible location of the DIRC expansion volume on the left side, corresponding to the internal readout option using a focusing lens.

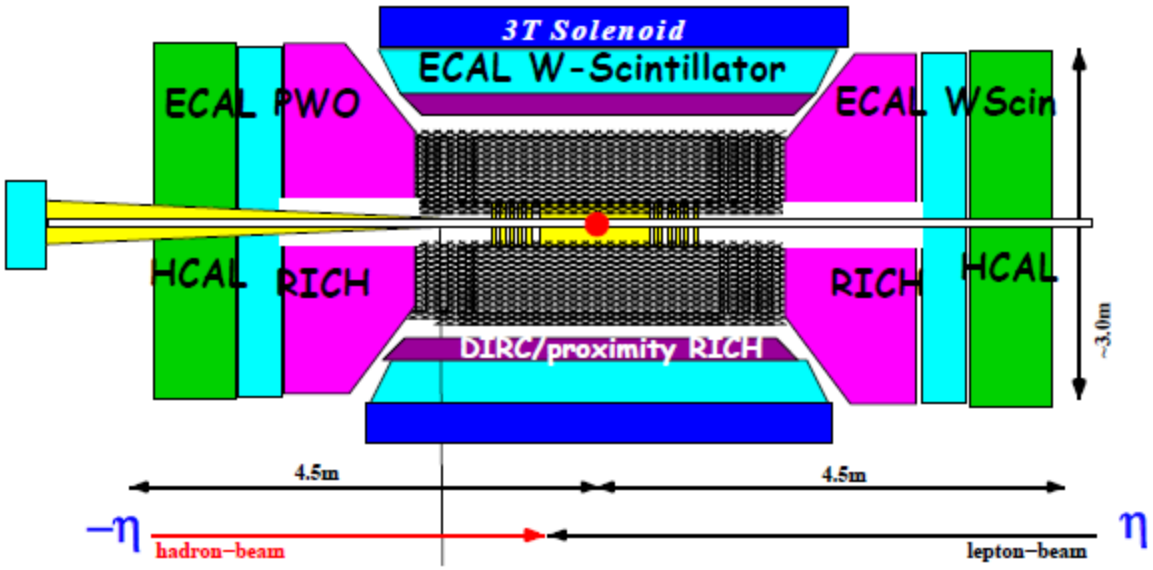

Figure 11: Side view of the BNL central detector based on a 3T solenoid (the iron yoke for the flux return is not shown). This layout is compatible with the internal readout option for the DIRC.

2.2 Brief overview of PID options

The EIC central detector will be required to provide e/π and π/K discrimination over a wide momentum range. The most compact solution is provided by DIRC technology, although an aerogel RICH could also be used (however, it is worth noting that, for instance, LHCb is considering replacing its aerogel RICH with the TORCH detector - essentially a time-of-propagation DIRC). Nevertheless, the state-of-the-art, as represented by the BaBar DIRC, offers performance that would be marginal for the EIC, in particular at forward angles. The most appealing option to address this issue is by improving the DIRC momentum coverage, which is the main topic of the proposed R&D.

An alternative would be to use a supplementary gas Cherenkov. This could be a simple threshold device or a RICH, and one could even imagine a dual-radiator device, combining the gas and aerogel options. But in all cases one has to pay a hefty price in terms of radial space. The simplest and smallest device, a threshold gas Cherenkov, could extend the momentum coverage up to 9 GeV/*c*, but would add at least 70 cm for the gas radiator, and would require space for readout beyond that. In total, the 0.1 m occupied by the DIRC would grow to almost 1 m. While one could at least consider this option in addition to a BaBar-type DIRC, reaching momenta of up to 4 GeV/*c*, even a small improvement in DIRC performance makes the tradeoff much less appealing. Since it currently seems feasible to reach a momentum coverage approaching 6 GeV/*c* at forward angles using focusing lenses, and perhaps also in other configurations, we no longer intend to make detailed simulations of ancillary detectors. We will instead spend that effort into broadening our simulation effort of the various DIRC readout options, both inside and outside of the magnetic field.

2.3 Solenoid options

Most superconducting detector solenoids today employ an iron yoke for the flux return, which encapsulates the detector and the endcaps. But an alternative has recently emerged. Dual solenoids have been used for some time in smaller applications, including the magnet to be used for the sensor tests in this proposal. However, the 4th detector concept for the ILC suggested the use of such a device for a large detector, which prompted the group at JLab to investigate its application to the EIC. While the pros and cons of various solenoid options go beyond the scope of this proposal, it does have some potential impact on various subsystems and sensors. From this point of view, the main difference is that the dual solenoid provides much easier access, both *in situ* and during maintenance. The main features of a dual solenoid are shown in Fig. 10. As will be discussed in section 2.5 below, the gaps in the endcap coils not only allow easy access to the calorimeter sensors, which could be placed outside of the magnetic field, but also make it possible to extend narrow detectors like a DIRC through the encap. Almost equally important is the additional space in the corners making where one would naturally place various readout systems, and perhaps cooling elements for sensors. The large gap between the outer solenoid and the endcap shown in Fig. 10 is also a useful feature, as sensors in the interior can be reached without disassembling the whole detector. And should one decide to do that, the light frame can be moved with much greater ease. These considerations could impact the discussion on the suitability of using different types of sensors throughout the detector.

2.4 DIRC configurations with readout inside of the solenoid

This configuration, shown in Fig. 10, has been the baseline for our simulation efforts, serving as a proof-of-concept. Indeed, it offers several advantages. It is the same technology that is being used for PANDA, which creates synergies with both hardware and software efforts at GSI. It allows for shorter, and cheaper, bars. It does not create integration problems in the endcap. There are, however, also challenges. First, using traditional lenses with air gaps, the photon yield drops as one approaches 90 degrees. To address this issue, a lens with a high index of refraction was introduced, and this kind of lens will be developed further within the framework of the proposed R&D effort. The other limitation is on the ability of the sensors to operate within the 3T field of the central solenoid, which is too high for traditional MCP-PMTs. While we are not proposing development of new sensors, we are planning to conduct tests in high magnetic fields of new, 3 and 5 micron pore-size MCP-PMTs to determine whether they would be suitable for this application. We will also test a number of SiPMs, to guide further development - even though the models available today are too noisy for DIRC applications (unless perhaps they can be cooled and a narrow trigger gate applied). Finally, the internal readout also limits the size of the expansion volume for the readout "camera," which should be no more than about 30 cm long and 20 cm high. This has guided our initial choices for the expansion volume geometry.

2.5 DIRC configurations with readout outside of the solenoid

Following the recommendations of the advisory committee, we will also investigate the option of placing the expansion volume outside of the endcap. This would be made easier by the use of an iron-free solenoid, where there are natural gaps between the relatively thin endcap coils into which the bars can fit, than if one has to penetrate the iron yoke around a 3T solenoid. Nevertheless, this would still require longer bars and a good solution for the encap, which would either be divided into two parts by the DIRC bars or, as shown in Fig. 12, will be boxed in by the electromagnetic calorimeter.

The longer bars would naturally favor a solution based on plates, *i.e.*, wide bars in which the number of bounces can be reconstructed exactly by use of precision timing. Such an approach has been pursued by the Belle-II iTOP, but the EIC DIRC could combine the time-of-propagation with good spatial resolution. Moving the readout to the outside would greatly reduce the requirements on compactness of the expansion volume and magnetic-field tolerance of the sensors. It would also give easier access to the sensors and front-end electronics if they would need replacement, for instance due to radiation damage.

However, the impact on detector integration and potentially on the overall performance of the endcap detectors would be significant, and would have to be evaluated carefully. On the DIRC side, new reconstruction algorithms would have to be developed for use with plates, incorporating both timing and spatial information on equal footing. And while the greater width of the plates (20 - 40 cm *vs.* 3 - 4 cm for bars) offers a lower cost per unit length, it also reduces the azimuthal segmentation, the impact of which will require further studies.

For these reasons, it is natural to use the lens-based option as a proof-of-concept for a high-performance DIRC, both in initial simulation and prototyping. But we also plan to pursue the outside option, looking at mirror-based designs for the expansion volume, as well as at cylindrical lenses.

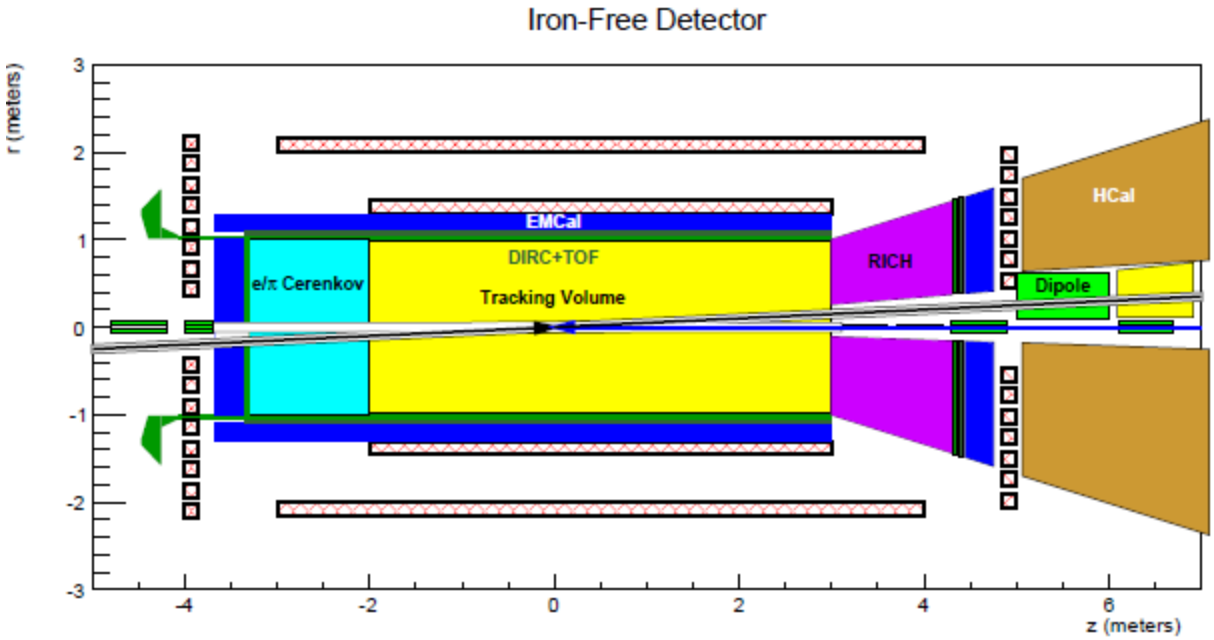

Figure 12: Top view of a central detector layout with DIRC bars (plates) penetrating the endcap and the expansion volume placed outside. Also shown is a possible hadronic calorimeter (perhaps with dual scintillation/Cherenkov readout for better muon identification).

2.6 Accelerator background

Accelerator backgrounds are an important consideration for the choice of detector and sensor technologies. This has recently been exemplified by the problems CMS has had with its lead-tungstate calorimeter. Problems with backgrounds were also experienced at other machines, such as HERA and PEP-II. For the EIC it will, however, be possible to design the interaction region such that synchrotron radiation is minimized, for instance by letting the electron beam pass along the axis of the solenoid while the ion beam crosses at an angle. Machine backgrounds for the two implementations are being worked on by the accelerator groups, and in the case of JLab, in collaboration with SLAC (Mike Sullivan). The findings at the simulation workshop in 2012, presented to the committee in the fall meeting, suggested that most of the problems at HERA were particular to that specific IR design. We are planning to work with the experts from both labs to keep up with the developments in background simulations, but considering that the DIRC sensors would be located in the corner of the detector where they would have minimum exposure, there do not seem to be any specific considerations related to the DIRC R&D. Thus, we feel that while radiation hardness is one of the aspects of sensors that need to be evaluated as more information comes in, we also think that pursuing tests of other aspects of sensor performance seems motivated unless there is a strong indication that a sensor type would be unsuitable for this particular application.

3. DIRC detectors

3.1 Principle

DIRC detectors are inherently 3D devices, measuring the image on the detector surface (x, y) and the time of arrival of each photon (t). If the distance to the detector surface is large compared with the bar size, as was the case in BaBar, no additional focusing is needed. Bringing the detector surface closer requires sensors with smaller pixels and some focusing optics. Fig. 13 shows a typical lens configuration, but focusing can also be done using mirrors.

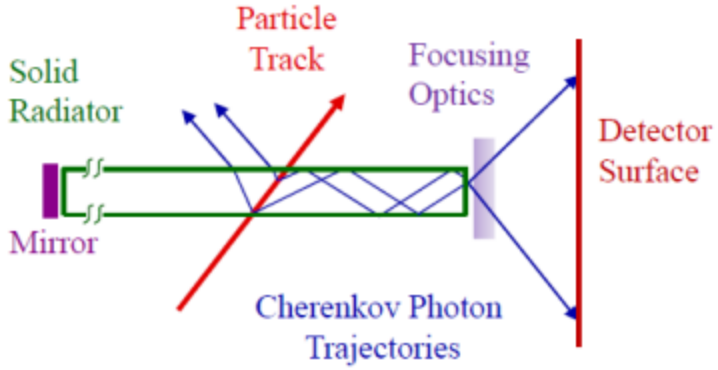

Figure 13: .Conceptual drawing of a DIRC with focusing optics.

Event reconstruction and particle identification for actual experiments can be done in different ways, but generally involve probabilistic approaches finding the maximum likelihood for a given hypothesis. However, from a design point of view it is easier to reconstruct and use the Cherenkov angle *(θ_c)* resolution, which can then serve as a figure of merit. This section will explain the contributions to the resolution and how they can be improved.

3.2 Contributions to the Cherenkov angle (θ_c) resolution

The expected PID performance of the DIRC is determined by the resolution in θ_c, the polar opening angle of Cherenkov light emitted from the particle traversing the detector. The angle θ_c is defined as $\cos\theta_c = 1/(n(\lambda)\beta)$, where $\beta = v/c$, v is the particle velocity and $n(\lambda)$ is the index of refraction of the material. In a dispersive medium, the latter is a function of λ, the wavelength of the Cherenkov photon.

The uncertainty of the Cherenkov angle for a particle track, σ_c^{track}, behaves as

$$(\sigma_c^{track})^2 = (\sigma_c^{photon}/\sqrt{N_{p.e.}})^2 + (\sigma^{track})^2,$$

where $N_{p.e.}$ is the number of detected photoelectrons and σ_c^{photon} is the single-photon Cherenkov angle resolution. The last term, σ^{track}, is the uncertainty of the track direction in the DIRC, dominated by multiple scattering and the resolution of the tracking detectors.

The single-photon Cherenkov angle resolution σ_c^{photon} can be calculated as

$$\sigma_c^{photon} = \sqrt{(\sigma_c^{2\,pixel} + \sigma_c^{2\,bar} + \sigma_c^{2\,imperfections} + \sigma_c^{2\,chromatic}}$$

where σ_c^{pixel} is the contribution from the detector pixel size, σ_c^{bar} is the uncertainty due to optical aberration and imaging errors, $\sigma_c^{imperfections}$ is the uncertainty due to bar imperfections (such as non-squareness), and $\sigma_c^{chromatic}$ is the uncertainty in the photon production angle due to the dispersion n(λ) of the fused silica material.

The readout "camera" consists of an expansion volume (EV) with attached sensors. The purpose of the expansion volume is to project a spatial image of the Cherenkov light from the DIRC bar onto the sensors. Using sensors with a smaller pixel size makes it possible to reduce the size of the expansion volume, or to improve the spatial resolution of the image. The size of the expansion volume can also be reduced by introducing active focusing elements (lenses or mirrors), although careful design and testing is required to minimize photon losses.

The size of the expansion volume planned for the PANDA barrel DIRC is 30 cm, both radially and along the beam axis, while the FDIRC that was planned for SuperB had a radius of 56 cm and a length of 22 cm. Due to its large radius, the SuperB EV would be challenging to integrate inside the EIC detector. Since an important goal of the R&D is to improve the DIRC performance beyond state-of-the-art, and there is a tradeoff between size and resolution, we expect the EIC expansion volume to be comparable to, or only a little smaller than the one planned for PANDA.

The next generation of sensors that will be used in the EIC DIRC needs to have a large number of small pixels and a high tolerance to magnetic fields (if they are mounted inside the field of the detector solenoid). However, for the proposed R&D it is cheaper and more efficient to use two sets of sensors each with a specific purpose. One set will provide a sufficient number of pixels for use with the expansion volume prototype to optimize the reconstruction of the projected image (MaPMTs), while the other set represents technologies expected to have a high magnetic-field tolerance (MCP-PMTs and SiPMs). Here, the focus will be on testing the performance of the sensor in the field.

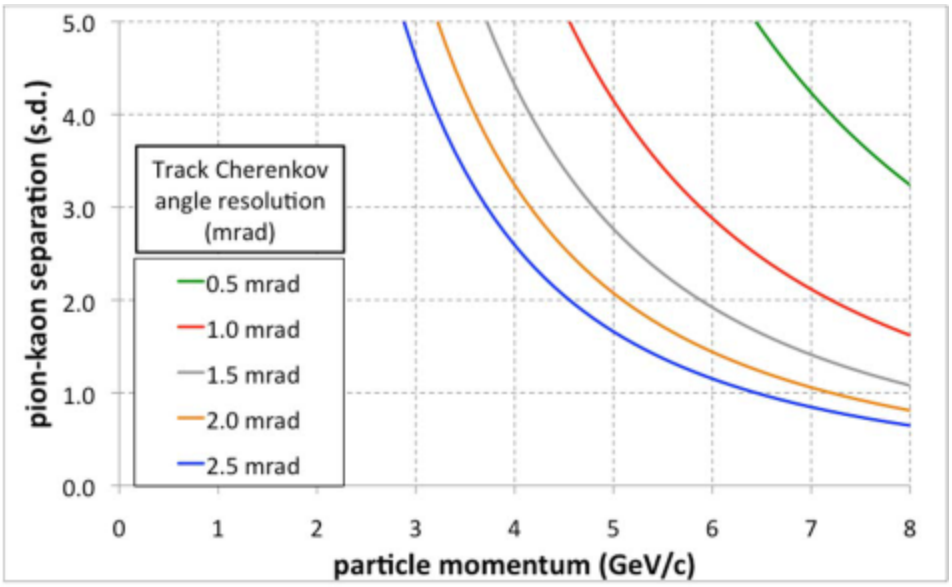

Figure 14: In order to have 3σ π/K separation at at 6 GeV/c one needs to reach a θ_c resolution of 1 mrad.

3.3 Adaptation to EIC requirements

The primary goal of developing a high-performance "Super-DIRC" is to have a compact device that can satisfy the PID requirements of the EIC without the need for a supplementary gas Cherenkov detector. Figure 14 shows how an increased momentum range for π/K separation translates into Cherenkov angle resolution. In an EIC, the pion background for kaons varies with reaction channel and kinematics, but is typically about 3:1. The usual 3σ criterion thus seems relevant. Achieving 3σ separation using radiator bars of fused silica would require a Cherenkov angle resolution of 1.3 mrad at 5 GeV/*c* and 1.0 mrad at 6 GeV/*c*. Achieving this resolution assumes that the central tracker will be able to provide an angular resolution at the mrad level (*i.e.*, comparable to the CLAS12 forward detector).

As suggested by the equations above, there are four ways of improving the Cherenkov angle resolution:

1. Reducing the size of the image from the DIRC bar using focusing optics.
2. Reducing the pixel size of the readout to better resolve the image.
3. Improving the photon yield and collection (various methods).
4. Reducing the effect of chromaticity (n = n(λ)) through precise timing or wavelength filters.

In this proposal we will study all four. A brief description of each point is given below.

3.3.1 Size of expansion volume

The required depth of the expansion volume is given by the size of the detector pixels, the size of the bar image after focusing, and the desired Cherenkov angle (θ_c) resolution. In order to reduce the EV size and to simplify operations, the water used in BaBar can be replaced with mineral oil or fused silica. The latter would be the preferred choice for the EIC.

In the EIC design we will try to improve performance while maintaining a compact size EV by introducing an active focusing element, such as a lens (or mirror). However, a compact design along the lines of

Belle-II, relying on precise timing while sacrificing spatial image resolution, would be unlikely to fulfill the requirements of the EIC.

3.3.2 Small-pixel readout

A small pixel size is essential for reaching the desired spatial resolution. To test the performance in a prototype, a sufficient number of channels is required. The most economical way of achieving this is to use multi-pixel PMTs such as the Hamamatsu R11265-103-M64 (64 pixels), of which four have been procured for the prototype.

3.3.3 Increasing the photon yield

The most straightforward way to improve the photon yield is to increase the bar thickness. This does not impose any additional manufacturing complications but adds to the thickness of material in front of the electromagnetic calorimeter. Simulations would be needed to study the impact of having bars with ≥0.2 r.l.. Instead, our effort is aimed at designing a focusing system that minimizes photon losses.

3.3.4 Sensor performance in magnetic fields

Tests will be performed using SiPMs (aka Geiger-mode Avalanche Photodiodes, G-APDs) and MCP-PMTs with small-diameter MCPs, such as the 3- and 5- μm pore-size Katod round, single-anode MCP-PMT. If the performance of the latter would be satisfactory for fields up to about 3T, production could eventually be undertaken of square multi-pixel PMTs with small-pore MCPs for use in the EIC detector. While SiPMs potentially could be less sensitive to magnetic fields, their high dark count rate (~ 1 MHz/cm^2 at room temperature) will require cooling to reach the desired performance.

The advisory committee suggested to join efforts with C. Zorn upon completion of his one-year, FY11 project to test improved, radiation-tolerant silicon photomultipliers. Consequently, the scope of the high magnetic-field testing of MCP-PMTs and SiPMs has been significantly expanded. To support this effort, as well as future EIC-related sensor tests, a dedicated test facility will be set up at JLab. A description of the facility and test plans can be found in section 4.3. The expanded sensor testing program has also brought additional collaborators to this proposal.

3.3.5 Precision timing

In a DIRC design with focusing optics and small-pixel readout the chromatic dispersion may no longer give a negligible contribution to the single-photon θ_c resolution. The focusing DIRC prototype at SLAC has shown that dispersion effects can be corrected by using fast timing at the 100-ps level, and this proposal thus aims to test the impact of timing close to that level. Should this prove not to be sufficient, more stringent timing requirements may be needed for the EIC DIRC, or wavelength filters can be applied to improve the single-photon resolution. The loss of photons due to the latter may, however, make the overall θ_c resolution for the track worse.

4. Proposed R&D

4.1 General Goals

The main goal of the proposed R&D is to investigate the possibility of, and provide a proof-of-concept for, improving the performance of DIRC detectors compared with state-of-the-art (BaBar), in particular at forward angles. In addition, we will also address the issue of integration with the EIC detector by looking at different focusing options (lenses, mirrors), bar widths, expansion volume locations (inside or outside of the solenoid field), and sensor performance. The goal is not to complete a detailed design of a DIRC for the EIC, but to address key issues through simulations, prototyping, and sensor tests, and establish what level of performance that could be reached in at least one configuration.

4.2 Detector simulations

We have completed several stages of simulation of the DIRC performance, using both GEANT4 and the dedicated *drcprop* ray-tracing code. The simulations include:

- Primary photo-statistics of the Cherenkov process.
- Chromatic effects on the Cherenkov light propagation and internal reflections in the bars, focussing elements, and expansion volume (EV).
- Quantum efficiency of the photodetectors.
- Time-of-propagation (TOP) of the Cherenkov photons from the track to the photo-cathode surface.

For the lens-based focusing readout detailed below, we have also implemented a reconstruction algorithm, based on the reconstruction approach developed for the PANDA DIRC, to quantify the resolution of the Cherenkov angle reconstruction for each configuration. In the reconstruction algorithm, a bundle of rays are generated near the end of the DIRC bar. The wave vectors fill the entire angular phase space of total internal reflection in the bar. After propagation of the rays through the lens and expansion volume, a look-up table is created associating each pixel of the photocathode surface with a specific unit wave vector $\hat{k}$. A separate look-up table is created for photons with 0, 1, 2, or 3 reflections off the sides, top, and bottom, of the expansion volume. The reconstruction of the detected pattern of Cherenkov photons proceeds as follows:

- For each detected photon, a Cherenkov angle θ_C is calculated from $cos\theta_C = \hat{k} \bullet \hat{p}$, where $\hat{p}$ is the track unit vector.
- The value of θ_C is histogrammed, including the 8-fold ambiguity from all possible reflections off the sides, top and bottom, and end of the DIRC bar.
- For each of the 8-fold choices of θ_C, a calculated Time-of-Propagation is subtracted from the simulated TOP and histogrammed.
- Separate timing and angle histograms are created for each number of reflections in the expansion volume. The histogrammed are summed for up to 2 reflections in the EV.
- An initial cut is placed on the timing histogram. This primarily selects the correct path of either direct propagation from track to EV, or reflection off the downstream end of the DIRC bar. This also helps to remove some of the ambiguity of reflections in the EV.

- A final cut is place on the θ_C histogram, and a gaussian plus polynomial fit is performed. The rms width of the gaussian fit, divided by the square root of the number of photo-electrons is the projected per-track resolution. In reconstructing data or pseudo data with a mixture of particles, the final cut position would be repeated for each particle hypothesis (pion, kaon, proton), based on the measured track momentum, and a likelihood assigned based on the number of photon candidates within the cut.

The progress of these studies is presented below.

4.2.1 GEANT

Figure 15 illustrates our initial simulations of the BaBar geometry with GEANT4. Following these results, we shifted our focus to simulation and reconstruction with the drcprop ray-tracing code, as discussed in section 4.2.2. Once the drcprop studies are complete, we will also simulate the resulting geometries using GEANT.

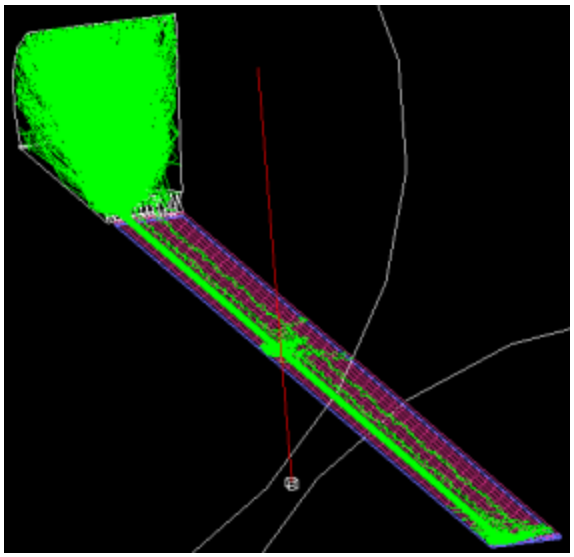

Figure 15: First study of a single BABAR DIRC element with GEANT4. The primary charged track is in red, with Cherenkov photons in green.

4.2.2 Configurations with expansion volume inside solenoid

The physics program for the EIC strongly motivates a full acceptance detector. To avoid interference with other detector elements, it is highly desirable to have a very compact focussing expansion volume inside the primary solenoid. To this end, we have simulated lens-based designs. With a short focal length of ~30 cm, we can achieve high resolution in a compact volume. Our sensor tests, detailed in section 4.3 will assess the feasibility of operating various photo-sensors in the fringe field of the central solenoid.

Our first study was with a two layer lens with a small airgap in between the layers. Although this gives good focussing properties, we found that the photon losses from internal reflection at the glass to air interface were too detrimental to the overall performance. We present additional discussion of lens design and prototyping in section 4.4.1. We present here a study of a two layer lens of high refractive index

materials, without an airgap. The first layer is F2G12 glass (n=1.620 @ 588 nm), the second layer is BK7G18 glass (n=1.519 @ 588 nm), and the expansion volume is fused silica. The interface between the two layers is spherical, with radius of curvature 30 mm. All other interfaces are flat. Two versions of the expansion volume are illustrated in Figures 16 and 17.

Most recently, we have started simulations with a three-layer lens, with a layer of PbF_2 sandwiched in between two BK7G18 layers. The radius of the BK7G18 to PbF2 interface is 37 mm, the radius of the PbF_2 to BK7G18 interface is 26 mm. This lens was designed to create a flatter focal surface, and possibly improve the transmission of large angle photons.

Figure 16: Reference expansion volume used for the drcprop simulations. The length of the box is 30 cm. The height of the box extends 15 cm above and 1 cm below the DIRC bar.

Figure 17: A prism with a flat vertical back wall is functionally similar to the box shown in Fig.16, but requires less space and material. Here. there are 1 cm steps both below and above the bar. Future optimizations will match the lens focal plane and the EV back plane to achieve the best single-photon resolution.

The Cherenkov angle resolution, as a function of the track angle, is displayed in Figure 18. These studies primarily focussed on improving the photon yields around 90°. The optimization of the focal plane and EV geometry is still ongoing. The two different expansion volume designs for the double-layer lens give essentially identical results. The triple-layer lens (with rectangular EV) also gives similar results, with some improvement around 80°. These studies were done assuming 3mm square pixels. A study with 1 mm pixels showed little improvement. Thus for the moment, we conclude that the 3 mm pixel size is optimized.

The mean number of photo-electrons per track is plotted in Figure 19. For both lenses, the dominant effect in Figure 19 is the ~1/sinθ track length in the DIRC bar. The box and trapezoid show identical behavior for the double lens. The triple lens shows improved light transmission.

We note (*e.g.*, Figure 2) that the typical momenta of particles produced in DIS increases at smaller angles. Although we are trying to maximize the DIRC performance over the entire angular range, having the best performance at forward angles is well matched to the physics challenge.

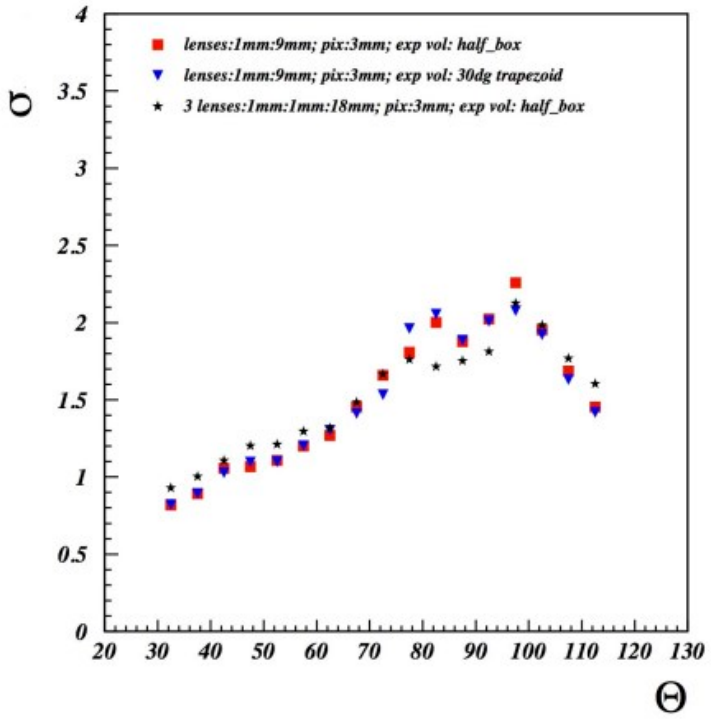

Figure 18: Per-track resolution obtained with a double-lens design with high-index of refraction. Double-layer lens: box EV (red squares), and trapezoid EV (blue triangles). Triple layer lens with box EV: black stars.

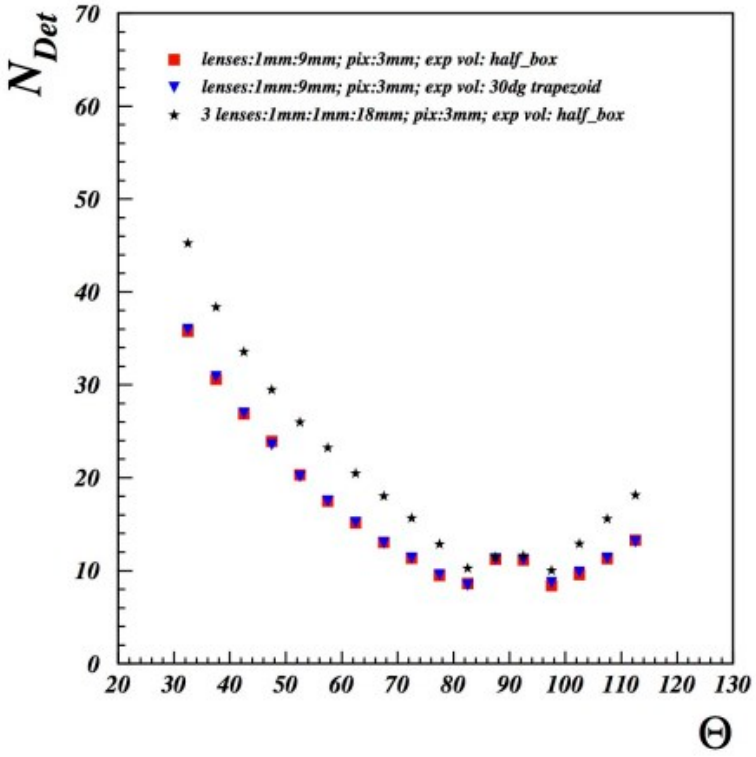

Figure 19: Number of detected photons for the same combinations of lenses and expansion volumes as in Fig. 18. The first iteration of a triple lens shows improvement over the double lens.

4.2.3 Configurations with expansion volume outside of solenoid

If the DIRC bars are extended through the compensation coils (Figure 12), then there is much greater flexibility in the design of the expansion volume and the choice of photo-sensors. We have done an initial simulation of the Cherenkov performance using the SuperB design for a mirror based expansion volume, as illustrated in Figure 20.

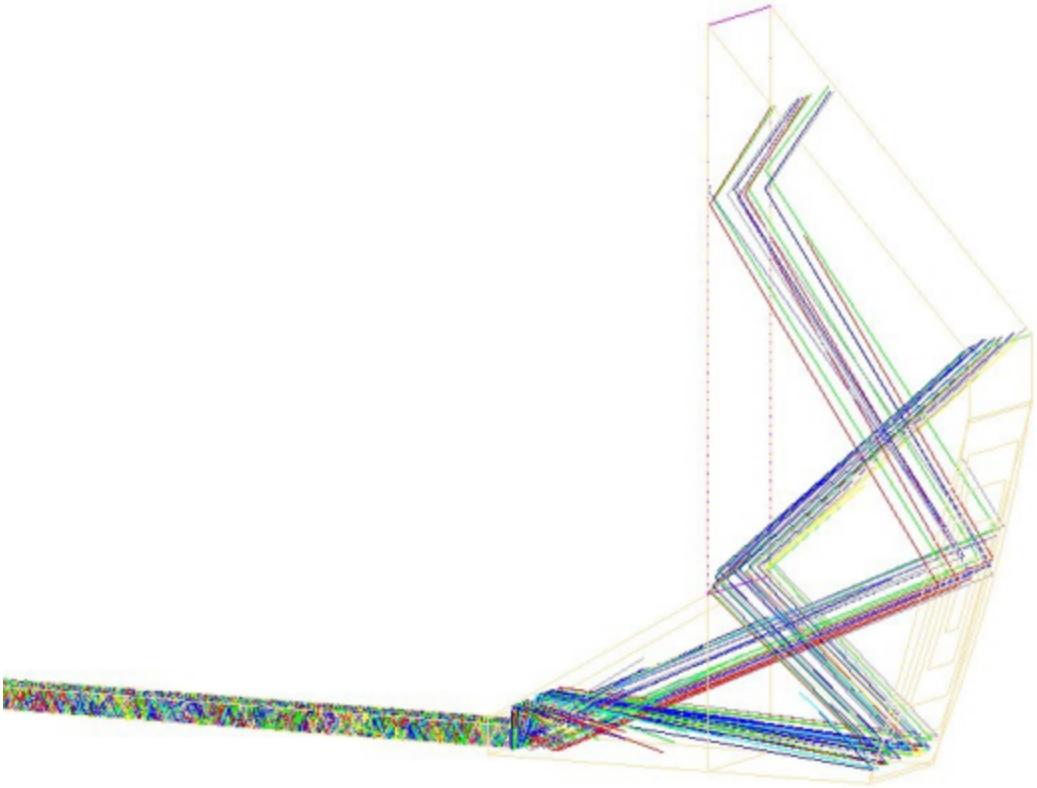

Figure 20: As a reference for simulations with mirror-based focusing and the expansion volume (EV) outside of the magnetic field, the FDIRC EV was implemented in drcprop. Reflections off the sides of the EV are suppressed in this image. Color coding is based on the number of reflections of the photons inside the DIRC bar (0-9, 10-19,... 90-99).

The image formation of the spherical surface of this Focussing DIRC (FDIRC) design is illustrated in Figure 21. In our future work we will study reconstruction resolution of this, or similar, designs.

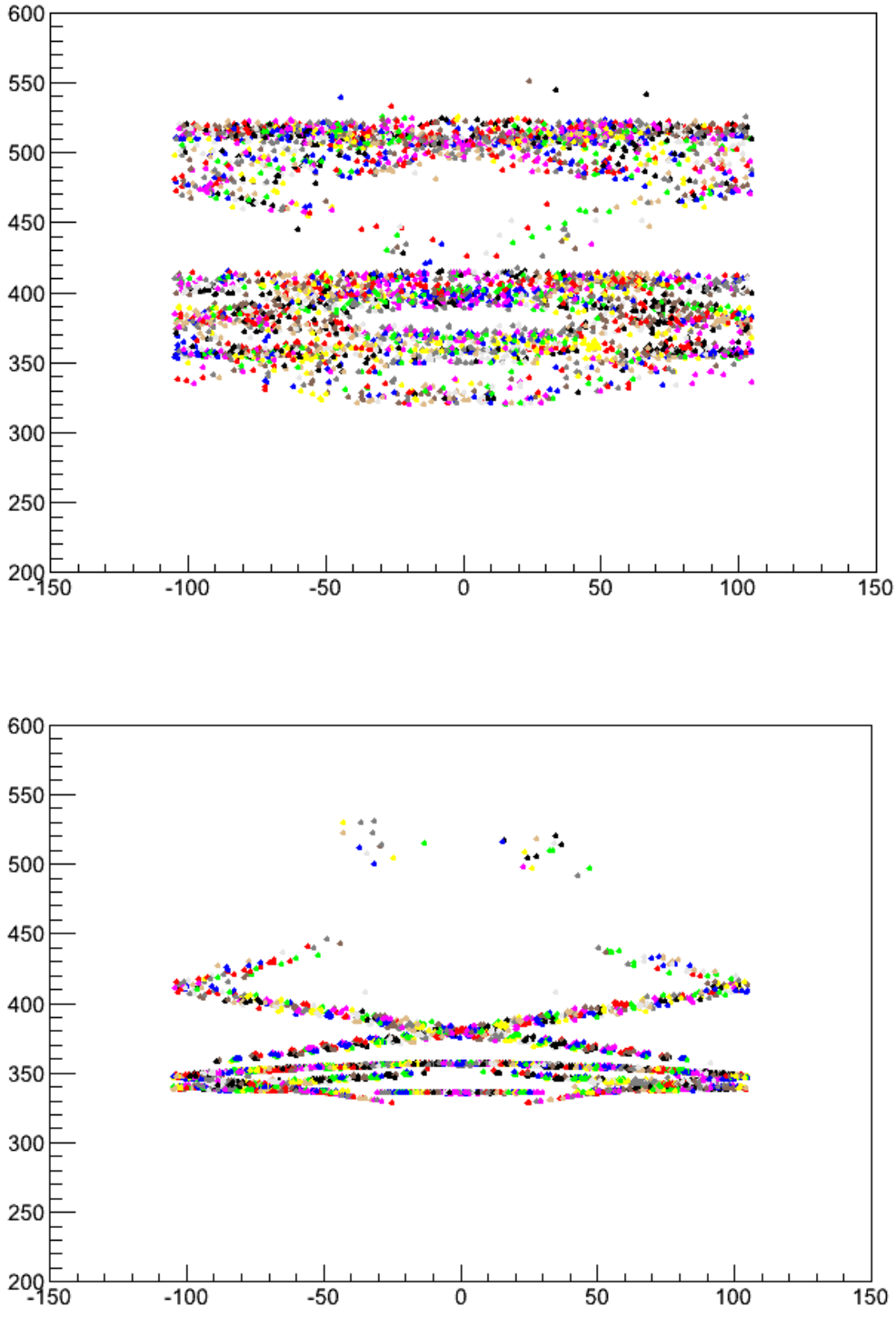

Figure 21: Distribution of photon impact points (in mm) on the photo-detector surface of the FDIRC design (Figure 20). All reflections on sides of EV are included. The top plot is a reference plot with all surfaces flat. The bottom plot has the spherical curvature of the back surface in Fig. 20. A total of 50,000 Cherenkov photons were generated from a 45° track for illustrative purposes. Color coding same as previous.

4.2.4 Prototype configuration

The prototype for tests in particle beams is expected to be based on the PANDA Barrel DIRC prototype built at GSI. The design will be modified to test the specific aspects of this R&D program, such as focusing options and fast timing.

A CAD drawing of the prototype used in 2012 for a PANDA Barrel DIRC test beam campaign at CERN is shown in Figure 22. A lifting table with a precision rotating stage is used to place the prototype into the beamline and adjust the position and polar angle of the radiator bar or plate relative to the beam. The radiator is placed into a holder on an X/Y stage which allows precision alignment of the radiator relative to the lens and expansion volume. A plastic fixture places the sensors into an array structure at the back wall of the expansion volume. The radiator, lens, expansion volume, and front-end readout electronics are placed in a light-tight box.

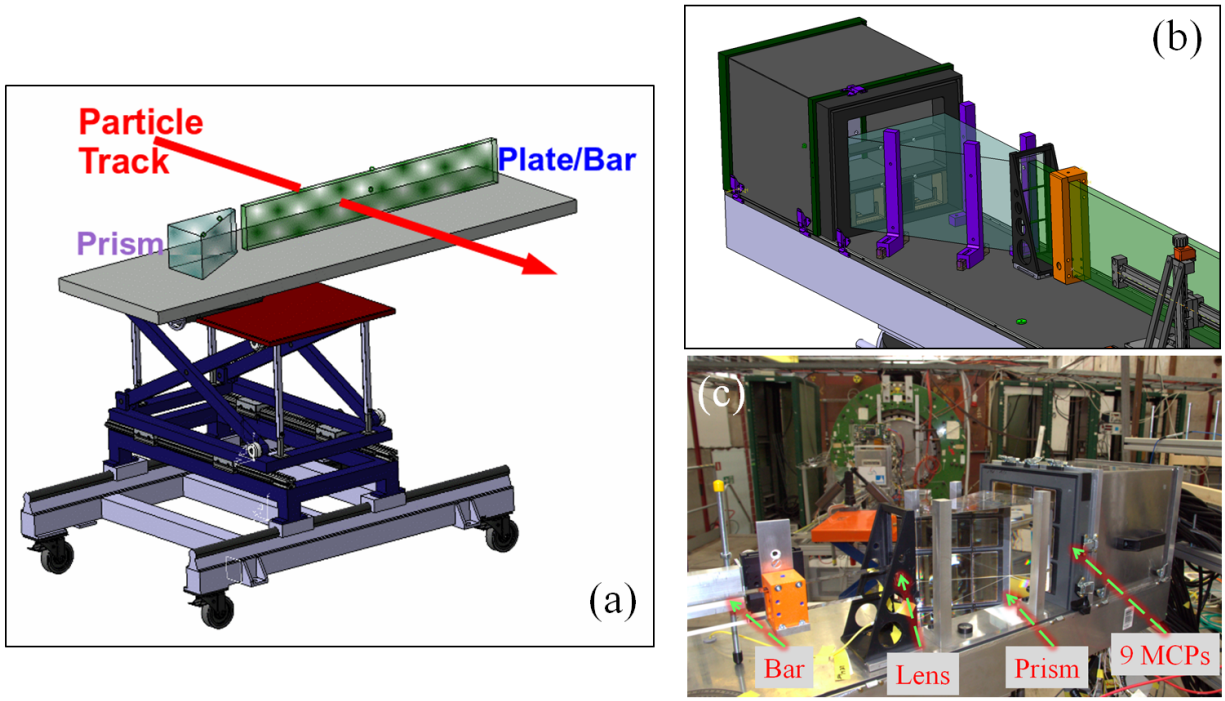

Figure 22: Layout of a possible DIRC prototype based on PANDA DIRC prototype design. Overview of components (a) and close-up of imaging region (b) showing a trapezoidal expansion volume (prism), focusing lens, and radiator plate. Photo of the prototype in a beamline at CERN in 2012 (c).

The advantage of the GSI prototype is modularity. Most of the components, such as the support table, radiator and lens holders, as well as the radiators and MCP-PMTs themselves, can be utilized for the EIC R&D. The prototype for the current R&D will modify this prototype by replacing the sensor fixture to allow placement of both MCP-PMTs and MaPMTs on the focal plane to study the focusing quality of different lens designs in detail. The solid fused silica prism used for the PANDA Barrel DIRC (length 30cm, width 17cm, top angle 30º) can be reused or replaced with a suitable compact expansion volume.

The readout electronics is equally modular and allows a partial replacement of the TRB2 with the newer TRB3 readout boards procured for this R&D effort.

Additional instrumentation, such as trigger counters, hodoscopes, and a time-of-flight system are available

in the PANDA Barrel DIRC group to measure beam properties.

4.3 Sensor tests

4.3.1 Gain studies at high-B field test facility at JLab

4.3.1.1 Facility description

Magnet; The main device of the test facility is the magnet. We will use a superconducting solenoid magnet that has become available at Jefferson Lab with the end of the 6-GeV program. The magnet provides a 4.7-T nominal field at its center point when it is energized at 534 A. The magnitude of the current is controlled and can be set to any desired value up to 534 A. Thus, the magnitude of the magnetic field can be flexibly increased or decreased while keeping the position of the probed device constant. This feature simplifies the design requirements for the test box which will hold the sensors. The major equipment necessary to operate the magnet such as cryostat, power supply, controls, holding frame, *etc.*, is also contributed by the Jefferson Lab. We request funding for hardware necessary to set up the magnet cooling system, such as pipes, valves, *etc*, in the new test lab where we will operate it.

Test Box; The design of a universal non-magnetic, light-tight test box is shown in Fig. 23. A first prototype has been manufactured by C. Zorn. It is made of non-magnetic material with dimensions 6" x 6" x 8". The tested sensor will be installed on an opto-mechanical mount that allows for rotation and translation of the sample relative to the magnetic field. The mount itself will be installed on an optical breadboard. The latter allows flexibility in using the box to test multiple/various configurations of sensors or add other elements to the test setup. The design of the lid of the box, with an inner sleeve, ensures a light-tight fit. We will use an LED as a light source. As the sensor will be rotated relative to the field, but the position of the LED will be fixed relative to the sensor, we will cover all the interior surface of the box with a diffuse white coating to allow the sensor to detect a signal independent of its orientation. Non-magnetic, light-tight fittings, mounted on the back side of the box, will be installed for the optical fiber input from the LED, high voltage, low voltage, and output signal. The box will be moved in and out of the magnet's bore using an aluminum rail mount. The design of the box is suitable for tests of various sensors such as SiPMs, MCP-PMTs, and also PS-PMTs. A test box of the same design, but with different dimensions, was already successfully used by one of us (C. Zorn) for SiPMs tests in magnetic fields up to 1 T at another facility. These previous tests have demonstrated that the proposed design indeed can provide the required functionality such as light tightness, operation in high magnetic field, and the ability to control the sensor orientation with respect to the magnetic field. Later in the project, we will add cooling and temperature control in the box when SiPMs are tested.

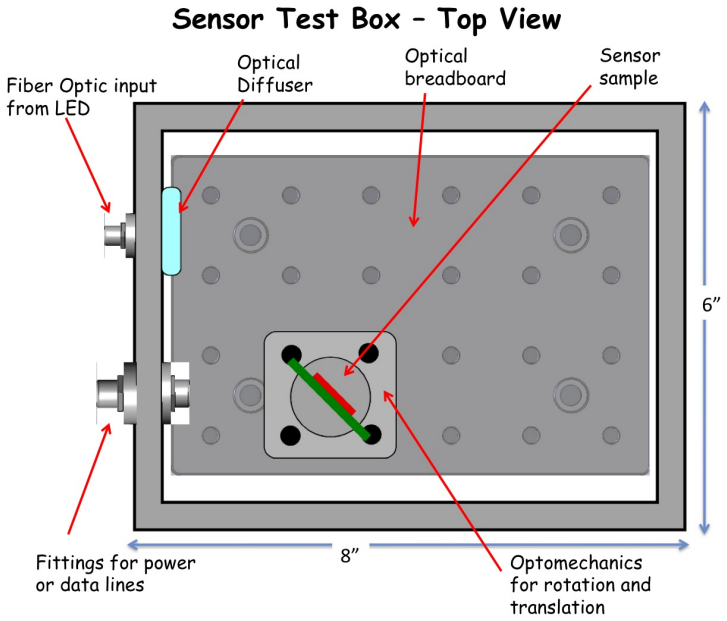

Figure 23: Design of a universal non-magnetic, light-tight box to be used for sensor tests in the high magnetic field of the DVCS solenoid magnet. Details are explained in the text.

Sensors; We will test the high-magnetic-field tolerance of SiPMs and MCP-PMTs. This includes the gain dependence on field magnitude, and gain dependence on field magnitude for various orientations of the sensor with respect to the field lines. We will use the MCP-PMT sensors that were already procured under this project during year one. As all of the tests that do not involve high magnetic fields will be done at GSI and there may be difficulties relocating the sensors from Germany to USA and/or back, we propose to acquire an additional set of SiPMs that is to be used for the magnetic-field tests only and will remain permanently at Jefferson Lab.

Electronics and data acquisition system (DAQ); Most of the readout electronics necessary for the sensor tests is general. Components such as amplifiers, discriminators, scalers, readout controller, and DAQ, are already available at Jefferson Lab. For the set of SiPMs which will be purchased for the high-field tests, we need to procure pulser, custom-built pre-amplifiers and a high-voltage supply.

Jefferson Lab contributes significantly to the project by providing equipment, facility infrastructure and technical support. The Laboratory has provided the magnet and the equipment that is necessary to operate it, most components of the readout electronics, and a laboratory space in a building with a direct supply of liquid helium, where the magnet and the test facility will be installed. The lab space will be available in July of 2013. The design and the construction of the test box has been done at Jefferson Lab by C. Zorn using funds from this project in year two. The equipment budget requested here for years three and four will allow Jefferson Lab to procure hardware to setup the cooling system of the magnet, several SiPM sensors

for the high B-field tests, fast pulser, LEDs, fiber optics, custom preamplifiers, and HV supply.

4.3.1.2 Planned tests and Procedures

The primary goal of the tests is to evaluate the performance of two types of sensors, SiPMs and MCP-PMTs, in magnetic field of up to 4.7 T and under single photon detection. At fixed temperature, we will map the gain of each sensor at various magnetic field magnitudes and orientations of the sensor's plate relative to the field lines. The latter will be achieved by rotating the box externally around an axis parallel to the magnetic field, and by rotating the sensor around an axis perpendicular to the field using the optomechanics in the dark box.

The initial setup of the electronics, readout, and the measurement procedure will be done at 0 B-field. For validation, we will evaluate the gain of an original Hall-D SiPM (in and out of magnetic field) that has been already measured by C. Zorn.

Once installed in the light-tight box, the sensor will be illuminated by photons originating from a light emitting diode (LED). The intensity of the LED will be controlled by a fast pulser. The light pulse will be driven into the box through an optical fiber. The stability of the light intensity will be monitored with a reference magnetically immune photodetector installed in the box. To ensure that the setup is operated in single-photon mode, we will run the pulser at 5% − 10% single-photon hit probability.

For each type of sensor, at 0 B-field, we will first establish the gain-voltage curve and determine the operating voltage, V_{op}. The charge output of the sensor will be recorded by an analog-to-digital converter (ADC). The gain will be estimated from the mean value of the single-photoelectron peak on the ADC after pedestal subtraction. For each type of sensor the gate width for the ADC will be adjusted so that after-pulsing is minimized.

SiPMs: We will first test Hamamatsu S11064-050P 4×4 arrays of 3×3 mm^2 50 μm SiPMs and at room temperature. Dark current rate as a function of reversed voltage will be measured by fully masking the sensor. Later in the project, we will test newer generation of SiPMs from several vendors, such as Hamamatsu, KETEK, SensL, AdvanSiD, STMicroelectronics, and Zecotek. We will extend the gain studies to sensors with various levels of radiation damage.

MCP-PMTs: We will first test Planacon photomultipliers already available at JLab. As newer sensors are procured from other vendors, such as Katod, the tests will be extended to include these as well. The goal is to determine the sensor's gain with an uncertainty of about 10% (less than 20% overall). Since the MCP-MPT gain varies significantly from hit to hit, the tests will be performed using a mask with a diameter of 0.25 - 0.5 mm placed in front of the photocathode. Previous studies of MCP-PMTs with pore sizes of 10-25 μm up to 2 T suggest that the amplitude of the output signal deteriorates due to the effect of the magnetic field on the trajectory of the avalanche electrons. These studies have shown that gain loss is smaller for smaller-diameter sensors. In addition to introducing small-diameter MCPs (our focus will be on

sensors with pore size in the range of 3 - 5 μm), a partial compensation of the loss of signal can be achieved by increasing the high voltage on the PMTs above the nominal working high voltage. Once the sensor is placed in magnetic field, we will scan the gain for voltages from V_{op} to V_{max}, where V_{max} is the maximum voltage set by the manufacturer. Thus, we will also establish the most optimal working high voltages to operate the MCP-PMTs for various strengths of magnetic field.

As the wavelength of the incident light affects the kinetic energy of the photoelectron and the kinetic energy is not affected by the magnetic field, we do not expect the response of the sensor in different magnetic fields to also vary with incident light wavelength. However, as we determine the most optimal working voltage for the sensor, and that may depend on the field magnitude, there may be wave-length dependent effects. In order to study any such effects, we will initially use only two types of light: blue and green. If we find that the response of the sensor in various fields also depends on the source wavelength, we will extend the tests to include wavelength dependence.

4.3.1.3 Broader impact

A high-magnetic field testing facility for sensor studies is of interest to a broad community. Currently, there is no research facility providing magnetic fields above 2 T. In order to test sensors in higher fields, one needs to negotiate access to magnets at clinical facilities. The latter have two aspects of inflexibility. First, access is not readily available and, if granted, it is very limited. Second, clinical magnets operate at fixed current, so that evaluating the sensor response over a range of magnetic fields requires complicated design solutions. For example, the probed sensor must be moved within the magnet in order to access locations with different field strength than the nominal one, and the setup must provide means to measure the field at the location of the sample. The ability to control the strength of the magnetic field in our setup is, thus, a great advantage. The relatively large diameter of the central bore of the magnet allows for the design of a universal light-tight box which can house sensors of various geometry and size. Once established, we envision that the high-magnetic field testing facility at Jefferson Lab will have a long-lasting value for sensor studies also beyond nuclear-physics applications, with mutual benefits. For instance, there is a growing interest to use SiPMs as readout elements in scintillator-based positron emission tomography (PET), particularly for small-animal or organ-specific imaging. The feasibility of SiPMs for such systems is currently ongoing. Specifically, a high B-field sensor testing facility can be useful for the development of combined PET/MRI scanners that use SiPMs.

4.3.2 Timing studies at GSI

A data acquisition system will be set up at GSI for timing studies of MCP-PMTs. The Trigger and Readout Board 3 (TRB3), shown in Fig. 24, which was designed at GSI, will be integrated into the TRB-net to connect the TRB readout boards to a desktop computer.

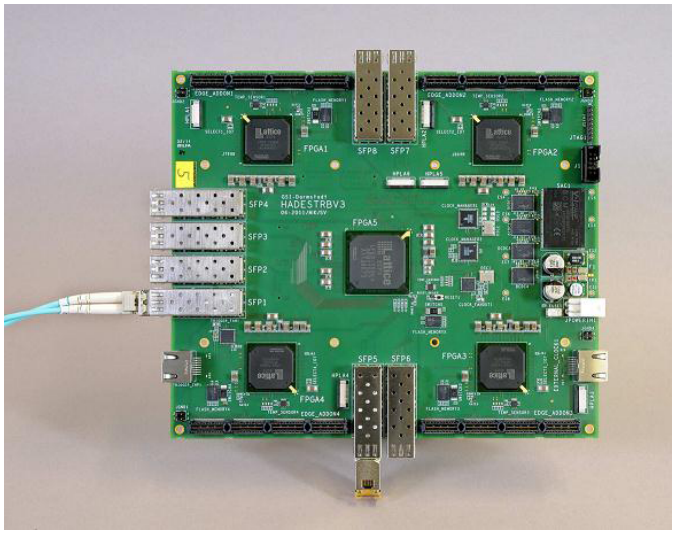

Figure 24: Trigger Readout Board 3 with four FPGA holding 256 TDC channels. A fifth FPGA is for communications.

The sensor is connected via an optional adapter board to a compact front-end board which amplifies and converts the analog signal into a digital signal that is plugged into a add-on card on top of the TRB3. Several choices for the front-end board design exist, including one based on the NINO chip or one using custom ASICs (e.g. the PADIWA chip). The adapter board for the Hamamatsu R11265-103-M64 MaPMT and a custom-designed set of PADIWA chips are part of the proposed procurement in year 3 and 4.

The time resolution for 256 channels of one TRB3 will be better than 20 ps. Together with an existing laser system (PiLas, 405 nm) the time resolution of various MCP-PMTs and MaPMTs can be determined. An example of the Hamamatsu R11265-103-M64 MaPMT, purchased for the EIC DIRC R&D, is shown in Fig. 25. It has a size of 26.2 mm × 26.2 mm, a nominal gain of 10^6, 8x8 anodes, corresponding to a pixel size of about 3 mm, and an active area ratio of 77%.

The measurements will profit from the experience with the TRB2 and TRB3 readout boards gained by the GSI group in the context of the PANDA DIRC R&D. For a test of SiPMs a dark box was prepared and measurements with an existing VME DAQ systems can be started. The capability to cool down the sensors down to temperatures of -20° C will be added in the near future as part of the proposed procurement.

Figure 25: Hamamatsu R11265-103-M64 MaPMT as delivered.

4.3.3 Radiation hardness

The determination of radiation levels and the radiation hardness of material, sensors, and electronic parts is an important issue. FPGA based TDCs close to the detector and SiPM sensors need special attention. Results of studies made under previous R&D, by C. Zorn *et al.*, have shown that both dark rate and dark current increase linearly as a function of total neutron fluence and the damage does not depend on the temperature or operating voltage. Part of the acute damage can be recovered by increasing the temperature of the damaged unit during non-irradiated periods. There is hope that the new generation of SiPMs with metal resistors are more radiation hard compared to the old generation with poly silicon resistors. The latter are illustrated in Figure 26. Radiation hardness tests of SiPMs within the PANDA-TOF project, which will take place at PNPI Petersburg, Russia, can be used to measure candidates for the EIC. An independent study of radiation tolerance of SiPMs is also being done at Jefferson Laboratory by C. Zorn.

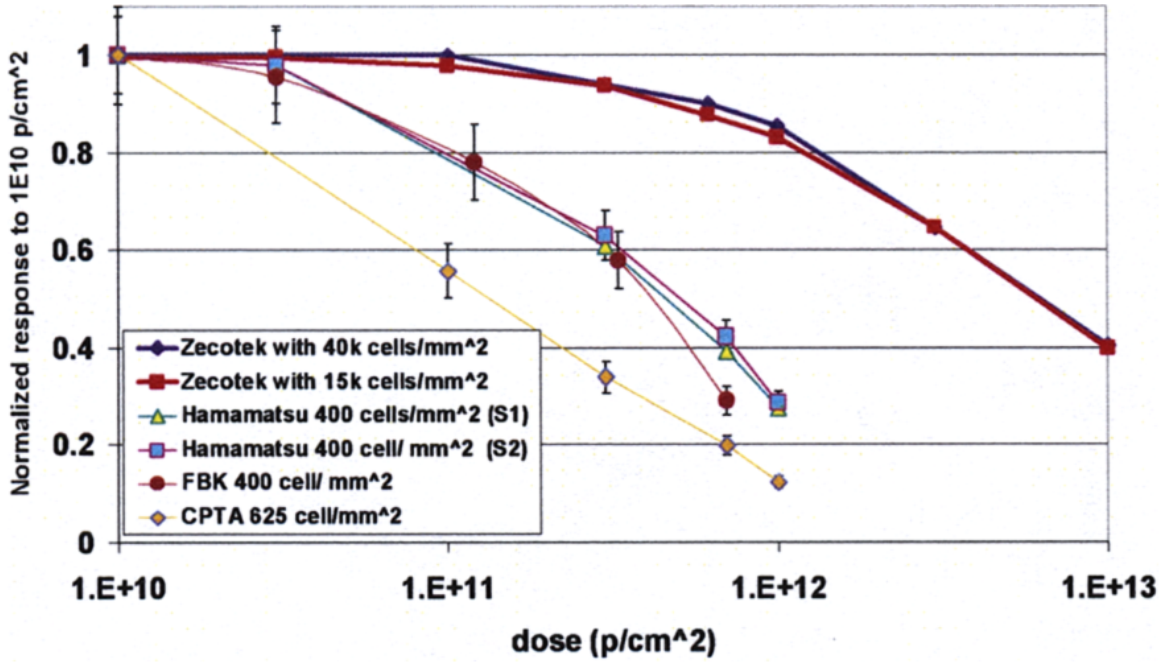

Figure 26: Radiation hardness of different SiPMs from Heering *et al.*, IEEE NS SCR 2008 NS-12.

4.4 Prototyping

4.4.1 Lens with high refractive index

Already a simple plano convex lens made of fused silica and a air gap between lens and expansion volume produces a focused image of the Cherenkov image. However, due to the refractive index jump at the airgap many photons are reflected back due to Fresnel scattering, especially, for large angles between photon and surface normal vector. Anti reflective coating might help and is worthwhile to be studied. Such a single lens produces, however, a non flat focal plane. It is better to fill the air gap with a material which acts as a defocusing lens shaping the focal plane. Since the radiator bar and the expansion volume have a low refractive index, the focussing and defocusing lens should have a refractive index which is different and larger than that of the transporting medium (radiator and expansion box). The combination of a focussing and defocusing lens allows to have a flat focal plane up to polar photon angles of 40 degree. Unfortunately, optical glasses with high refractive index, especially radiation hard glasses, cut off the UV photon <400 nm. Lead fluoride PbF_2, has a high refractive index (nd=1.77), is radiation hard and has a cut off at 300 nm. With this material as focussing lens and eg. BK7G18 (nd=1.52, radiation hard) as defocusing lens a flat focal plane at a distance of 300mm can be achieved. Prototyping a doublet lens from PbF_2 and BK7G18 will show, if PbF_2 is a mechanically usable lens material.

4.4.2 Compact expansion volume

A compact expansion volume, when made from fused silica, keeps costs reasonable low and alleviates the maintenance. It allows photon detectors with smaller pixel size and thus lower costs. An existing fused

silica prism at GSI can be used for prototype measurements.

4.4.4 In-beam tests

The primary goals of the tests of prototypes with particle beams are

- determination of the photon yield per particle;
- determination of the single photon Cherenkov angle resolution;
- demonstration of the effect of fast timing on the Cherenkov angle reconstruction.

These tests are best performed in a hadron particle beam with momenta between 3 and 8 GeV/c. An example of such a beam line is the T9 area at the CERN PS. Successful tests of the PANDA Barrel DIRC prototype were performed there in 2011 and 2012. A lower momentum hadronic beam was available for DIRC tests at GSI in 2011. However, due to shutdown plans at CERN and at GSI no beam time is available in 2013. Other possible beam lines, such as DESY, are also closed in 2013 for upgrades or due to budget concerns. This requires a postponement of the planned in-beam tests for the EIC DIRC R&D effort. The procurement plan has been adjusted accordingly.

The updated plan for in-beams tests is based on the beam time planning for the PANDA Barrel DIRC detector, which makes the best possible use of the synergy between the two DIRC R&D programs. The PANDA Barrel DIRC collaboration plans a beam time application at GSI for the first or second quarter of 2014 and a beam time application at CERN for the summer or fall of 2014. The EIC DIRC in-beam tests will be coordinated with the GSI PANDA group and performed during the allocated PANDA Barrel DIRC beam time.

4.5 Synergies

The hardware R&D makes substantial use of synergies with the PANDA DIRC detector development, both in terms of available hardware components and experience gained during the production of prototypes for bars, plates, and expansion volumes.

An example is the use of radiator bars made from synthetic fused silica. The production of a bar with optical quality sufficient for the EIC DIRC prototype would require a minimum of 4 - 8 bars to be produced at a cost of approximately $25k - $30k per bar. However, a number of prototype bars were produced for the PANDA Barrel DIRC R&D at GSI. The EIC DIRC R&D will have access to one of the bars for a possible test beam run.

Another example is the test of photon sensors. The GSI group owns a $10k electronic pulser and a $15k fast laser pulser system (PiLas) with a FWHM timing jitter below 25 ps, required for measurements of the fast single photon timing for the EIC DIRC. The test of SiPMs will require the sensors to be cooled to between -10° and -25° C. For simple tests a Peltier-cooled setup will be constructed at a modest cost. For more detailed studies the R&D will make use of a $10k large cooling box owned by the GSI group.

A software package, drcprop, for ray-tracing Cherenkov photons in DIRC radiators, developed at GSI, has been ported to the JLab computing environment for EIC DIRC R&D.

The planned beam time applications of the PANDA DIRC group are expected to provide an opportunity for placing the EIC DIRC prototype into a particle beam at CERN or GSI in 2014.

5. R&D Timeline and Deliverables

5.1 Timeline

5.1.1 Year 1

Design and Simulation:

Studies of different expansion volume sizes, shapes, focusing designs, and radiator shapes, in terms of single photon resolution and light yield.

1. Implementation of initial prototype in stand-alone ray-tracing software, including:
    a. Polished fused silica bar
    b. Small 30-cm depth expansion volume
    c. Focusing lens
    d. Multi-pixel readout
2. Development of a reconstruction algorithm (bar geometry).

Hardware:

Preparation of setup for prototyping of focusing lens and expansion volume at GSI.

1. Procure DAQ hardware and MaPMTs for prototype development.

5.1.2 Year 2

Design and Simulation:

1. Simulation of an EIC DIRC with the readout camera inside the detector volume.
2. Design of a focusing lens with high refractive index (no air gap).
3. Investigate opportunities for e/π identification in the central EIC detector using a DIRC.
4. Determine the need for supplementary π/K identification based on estimated DIRC performance

Hardware:

1. Installation and setup of high magnetic field sensor testing facility at JLab.
2. Set up and test DAQ system for readout of MaPMTs (at GSI).

5.1.3 Year 3

Design and Simulation:

1. Simulation of an EIC DIRC with longer bars and readout camera outside of the detector volume.
2. Design of EV prototype.
3. Development of a reconstruction algorithm for fused silica plates (wide bars).
4. Initial implementation of the EIC DIRC in the full EIC detector.

Hardware:

1. Measurement of MCP-PMT and SiPM gain in magnetic fields up to 4.7 T.
2. Construction and characterization of a lens prototype.

5.1.4 Year 4

Design and Simulation:

1. Interaction between DIRC and other detector components.

    a. material budget
    b. optimize location
2. EIC DIRC performance for selected physics channels.

Hardware:

1. Measurement of MCP-PMT and SiPM gain in magnetic fields up to 4.7 T.
2. Construction of EV prototype.
3. Test performance of prototype with particle beam (if available).

5.2 Deliverables

5.2.1 Year 1

1. Simulation and reconstruction framework for DIRC prototype.
2. DIRC resolution studies and initial design of focusing lens and EV.

5.2.2 Year 2

1. Setup and commissioning of the high-B field sensor testing facility at JLab.
2. Performance evaluation of an EIC DIRC with internal readout.
3. Design of focusing lens with high index of refraction (no air gap).
4. Laser pulser test of DAQ and MaPMTs to be used for prototype at GSI.
5. Investigation of opportunities for e/π identification in the central EIC detector using a DIRC.
6. Investigation of needs for supplementary π/K identification based on estimated DIRC performance.

5.2.3 Year 3

1. Evaluation of MCP-PMT and SiPM response in magnetic fields up to 4.7 T.
2. Performance evaluation of an EIC DIRC with external readout.
3. Construction and characterization of the lens prototype.
4. Design and preparation for construction of the EV prototype.
5. Initial integration of a DIRC into the EIC detector.

5.2.4 Year 4

1. Evaluation of MCP-PMT and SiPM response in magnetic fields up to 4.7 T.
2. Construction of compact EV prototype.
3. In-beam test of complete prototype with lens, EV, and sensors (if test-beams are available).
4. Determination of Cherenkov angle resolution of prototype.
5. Comparison of photon yield for different multi-pixel sensors.
6. Performance evaluation of the DIRC in the EIC detector.

6. Management Plan

6.1 Funding Request and Budget

We request a total of $485k over a four year period, as indicated in the tables below. The tables list the budget broken down by category and recipient.

Budget

	Year 1	Year 2	Year 3	Year 4	*Total*
Postdoc (50%)	$53,290	$54,000	$55,200	$56,300	*$218,790*
Students	$8,300	$13,764	$13,764	$13,764	*$49,592*
Hardware	$41,970	$58,630	$27,000	$30,000	*$157,600*
Travel	$11,440	$13,606	$19,036	$14,936	*$59,018*
Total	*$115,000*	*$140,000*	*$115,000*	*$115,000*	*$485,000*

	Year 1	Year 2	Year 3	Year 4	Total
Old Dominion University	$53,290	$54,000	$55,200	$56,300	*$218,790*
Catholic University of America	$9,800	$8,300	$8,300	$8,300	*$34,700*
University of South Carolina		$7,606	$12,646	$7,606	*$27,858*
JLab and GSI (through a MoU)	$51,910	$70,094	$38,854	$42,794	*$203,652*
Total	*$115,000*	*$140,000*	*$115,000*	*$115,000*	*$485,000*

Comments

The postdoc and students funding includes university overhead. Matching funds are available for the postdoc. Travel costs include JLab and USC overhead. Hardware costs include JLab overhead. The larger travel budget for Year 3 mainly reflects the need to bring participants to work on the high-B field test facility.

6.2 Procurement

The procurement schedule has been redistributed over four years to reflect the new timeline of the proposal, aiming to reduce annual costs.

Year 1 (completed):

1. Four Hamamatsu R11265-103-64 MaPMTs (64 pixels each): $12.6k
2. HADES TRBv3 board (256 channels): $2.7k

Subtotal: $15.3k

Year 1 (in progress, delivery rolled over to Year 2):

1. Hamamatsu E11906 voltage dividers for the R11265-103-M64 MaPMTs: $2.6k
2. Adapter cards for connecting to the PADIWA cards used by the TRBv3 board: $2.5k
3. Cabling for MaPMTs, cards, and TRBv3 board: $0.5k
4. Temperature-controlled cool dark box for SiPM tests at GSI: $2k
5. One Katod type I 5-µm single-anode round MCP-PMT: $4k
6. Materials for CUA undergrad student (computer, etc): $1.5k

Subtotal: 13.1k

Year 1 total: $28.4k

Year 2:

1. One Katod type II 3-µm single-anode round MCP-PMT: $4.5k
2. Non-magnetic light-tight cool box for high-B sensor tests: $2k
3. Fast pulse generator for the high B-field tests (refurbished old model): $1k
4. High B-field testing equipment (LEDs, fiber optics): $1k
5. SiPMs preamplifiers and HV supply (high B-field tests): $4k
6. SiPMs from several manufacturers for tests at GSI and JLab: $7k
7. High-B field facility magnet installation and He supply: $14k

Total: $33.5k

Rolled over to Year 3: $10k (already paid out)

Year 3:

1. High-refractive-index lens for use with EV prototype: $15k
2. Initial components for EV prototype: $14k

Total: $29k

Year 4:

1. Compact EV prototype from solid fused silica: $21.5k

Total: $21.5k

Comments

Some costs are in Euro. A conversion rate of 1.3 USD per 1 Euro is assumed. Listed costs are direct.

6.3 Responsibilities

The proposal is a collaborative effort and most participating institutions will contribute to many aspects of the work outlined in section 5. Nevertheless, we have identified three main areas of responsibility.

1. Simulations, design, and integration of the DIRC into the EIC detector will be the primary responsibility of ODU, CUA, and JLab. To carry out these tasks, a postdoc (Helena Seraydaryan) has been hired by ODU, and undergraduate students will be hired each summer at CUA, the latter focusing on integration and overall detector performance.

2. Evaluation of the sensors performance in high magnetic fields will be the primary responsibility of USC and JLab. A graduate student (Tongtong Cao) and undergraduate students from USC will contribute to the installation of the test facility and will perform the sensor tests. A dedicated facility will be set up at Jefferson Lab under the lead of C. Zorn to perform these tests. JLab will provide the infrastructure, the magnet, most of the readout electronics, and the data acquisition.

3. GSI will have the primary responsibility for sensor timing test, development of the focusing optics, construction of the prototype, and in-beam testing.

The travel support will create opportunities to have yearly collaboration meetings. It will also allow the US partners to take part in the development of the hardware at GSI, and for the German partners participate in the activities of the EIC collaboration.